Cigolini C., M. Laiolo, G. Ulivieri, D. Coppola, M. Ripepe (2013) Radon mapping, automatic measurements and extremely high 222Rn emissions during the 2002–2007 eruptive scenarios at Stromboli volcano, JOURNAL OF VOLCANOLOGY AND GEOTHERMAL RESEARCH (ISSN:0377-0273), pp. 49- 65. Vol. 264.

http://dx.doi.org/10.1016/j.jvolgeores.2013.07.011
http://www.sciencedirect.com/science/article/pii/S037702731300231X

RADON MAPPING, AUTOMATIC MEASUREMENTS AND EXTREMELY HIGH ^{222}Rn EMISSIONS DURING THE 2002-2007 ERUPTIVE SCENARIOS AT STROMBOLI VOLCANO

Cigolini C.[1,3], Laiolo M.[1], Ulivieri G.[2], Coppola D.[1], Ripepe M.[2]

1 – Dipartimento di Scienze della Terra, Università di Torino,Via Valperga Caluso 35, 10125 Torino, Italy

2 - Dipartimento di Scienze della Terra, Università di Firenze, Via La Pira 4, 50121 Firenze, Italy

3 –NatRisk, Centro Interdipartimentale sui Rischi Naturali in Ambiente Montano e Collinare, Universita` degli Studi di Torino, Italy

Correspondig Author: Corrado Cigolini; Email: corrado.cigolini@unito.it; Phone: +39-011670-5107; Fax: +39-011670-5128

Abstract

We report additional radon data collected at Stromboli during 2002-2007. The whole data set of periodic measurements has been systematically analyzed to retrieve the values of background, threshold and anomaly for all the stations of the network. Maps of radon concentrations in space and time correlate with changes in volcanic activity. Higher radon emissions are essentially concentrated at summit stations and may also affect some stations located onto the summit-eastern sector of the cone (along the N60°E fracture zone), as well as two stations placed at the NE edge of Sciara del Fuoco. Most of these stations are well above their threshold values during effusive eruptions (namely 2002-2003 and 2007) due to the progressive structural adjustment of the volcano edifice coupled with the opening and resetting of the fracture network.

A two-year-long timeseries of automatic ^{222}Rn measurements (2005-2007) was analyzed together with local environmental parameters and selected geophysical data (on seismic tremor and infrasonic puffing). The data show good correlation between radon and the latter parameters

particularly during periods of high Strombolian activity (March-April 2006), and before the onset of the February 27, 2007 lava effusion (with radon emissions being well above 20,000 Bq/m^3).

Extremely high radon emissions (up to ~1.7 x 10^6 Bq/m^3) were recorded along the fractures of the SW crater during the first two months of the 2002-2003 effusive eruption. Very high radon emissions (up to ~470,000 Bq/m^3 for ^{222}Rn, and ~780,000 Bq/m^3 for ^{220}Rn, respectively) were also detected by the automatic measurements at the summit station during June 20-early July 2007: i.e., just prior the resuming of the Strombolian activity at summit craters. These data give us the opportunity to estimate the relative depths of the summit fractures during fracturing (being constrained between 200 and 310 m). This is in good agreement the hypocentral depths of the so called "hybrid events" and the source of the very long period seismic signals (VLP) localized at a depth of about 500 m a.s.l. below the upper-central part of the Sciara del Fuoco.

1. Introduction

Changes in the concentration of radon have been detected before and during the onset of volcanic eruptions, both explosive and effusive, and volcanically-related earthquakes. Radon is a chemically inert noble gas generated in a great variety of rocks and soils. In nature, it is essentially represented by the isotope ^{222}Rn (with a half life of 3.82 days) and it may easily permeate the rock pores and fractures and, in association with a carrier gas (water and carbon dioxide), can migrate to significant distances from the site of origin before its decay. Systematic measurements on the variations of gas radon are essentially related to its decay properties (since it is not a reactive element) and give reliable information on the dynamics of fluid transport processes and surface degassing in complex hydrothermal systems.

The first work on anomalous radon emissions, interpreted as precursory signals of volcanic eruptions, was published by Chirkov (1975) who studied the onset of the explosive activity at Karimsky volcano (Kamchatka). After his pioneer work, Cox (1980; 1983) and Thomas et al. (1986) reported positive radon anomalies prior changes in volcanic activity and seismicity at

Hawaii. Additional significant findings were presented by Segovia and Mena (1999) who concentrated their work on four explosive American stratovolcanoes (El Chichón and Popocatepel in Mexico, Poás in Costa Rica, and Cerro Negro in Nicaragua). They found a positive correlation between the increase in radon and the Volcanic Explosivity Index (VEI) of single eruptions. Their data show that the ratio peak Rn-values/mean quiescence Rn-values, may be as high as 22.6 for eruptions with VEI up 5 (i.e., the eruption of El Chichón on March 28, 1982) and up to 4-4.8 for eruptions with VEI < 2 at the above volcanoes.

At Somma-Vesuvius, Cigolini et al. (2001) used a network for radon monitoring to discriminate signals produced by regional earthquakes from those derived by the local volcanic seismicity. Burton et al. (2004) used radon to decode the geometry of a hidden fault at Mount Etna during a seismic crises of October, 2002. Cigolini et al. (2007) analyzed earthquake-volcano interactions at Stromboli volcano: radon anomalies may be coseismic, precursory, and may also occur with a time-delay in respect to the onset of major regional seismic events. Radon anomalies prior the onset of volcanic eruptions or changes in volcanic activity have been also reported in recent times (Connors et al., 1996; Alparone et al., 2005; Cigolini et al., 2005; Neri et al., 2006; Padilla et al., 2013). Piboule et al. (1990) found an excess of ^{210}Po (a daughter product of ^{222}Rn) in sediments of Lake Nyos (Cameroon) that were likely released with deadly CO_2 emissions. Su & Huh (2002) detected an increase of ^{210}Po deposited by the plume of Mayon prior to its last eruption. Lately, radon measurements have been systematically collected at several active volcanoes (Varley and Armienta, 2001; Williams-Jones et al., 2000; Hernandez et al., 2004; Giammanco et al., 2007). Radon ascent occurs essentially along faults or fractures, and it is controlled by bulk porosities and permeabilities (e.g., Cigolini, 2010). In volcanic and hydrothermal environments, its migration is ruled by convection and advection and is passively carried by water and carbon dioxide (e.g., Gauthier and Condomines, 1999). However, at the site-scale diffusion may also be effective (Duenas et al., 1997; Giammanco et al., 2007).

Recent automatic measurements have shown that environmental parameters are critical in modulating radon emissions (e.g., Pinault and Baurbon, 1996; Zimmer and Erzinger, 2003; Pérez et al., 2007; Cigolini et al., 2009; Laiolo et al., 2012) and CO_2 degassing (Viveiros et al., 2008; Carapezza et al., 2009; Rinaldi et al., 2012). In this paper we will report additional data collected during 2002-2007 at Stromboli volcano. In particular, we will focus our attention on processes that were not extensively treated in previous papers. In addition, we present a two-year-long timeseries of automatic measurements as well as some measurements on very high and extremely high radon emissions. Then, we will analyze the chronology of the techniques applied in radon monitoring at Stromboli within the last ten years, and discuss their use and efficiency in monitoring active volcanoes.

2. Stromboli volcano

Stromboli is an open-system active stratovolcano and its activity is considered as a reference case for classifying minor to intermediate volcanic eruptions (e.g., Newhall and Self, 1982). It is located in the southern Tyrrhenian sea, being the north-eastern island of the Aeolian arc (Fig. 1a). Its cone is built on a NE-SE normal fault with a moderate oblique component: the Stromboli-Panarea (SA) alignment. This structure is connected to the NNW-SSW trending Tindari-Letojanni fault that crosscuts eastern Sicily and the southern Tyrrhenian region (cf., Ventura et al., 1999; De Astis et al., 2003; Acocella and Neri, 2009). The volcano rises 924 m above sea level and was built during the last 100 kyr (Gillot and Keller, 1993) with its submerged part reaching a depth of about 2,000 m below sea level. The hydrothermal system of Stromboli volcano is essentially concentrated in the surrounding of the summit area (Finizola et al., 2002; 2003). However, the presence of thermal waters and vapors in the surrounding of the Stromboli village together with radon anomalies and low resistivity layers suggests the extension of the hydrothermal shell at lower altitudes (Carapezza et al., 2004; Cigolini et al., 2005; Revil et al., 2011).

The typically mild Strombolian activity occurs when magma reaches the summit crater vents (NE, central and SW, located at ~750 m a.s.l.), and releases gas-pressurized scoria jets (100 to 200 m in height) triggered by moderate and periodic explosions (every 10 to 20 min; e.g., Blackburn et al., 1976; Patrick et al., 2007). This activity may be occasionally replaced by lava flows and more energetic explosions with the eruption of larger volumes of scoria-bombs, blocks and ash, named "paroxysms". Their onset is usually accompanied by the ejection of eruptive columns with the projection of blocks of several tons that may reach the villages on the coast of the island (Barberi et al., 1993; Rosi et al., 2006; Pistolesi et al., 2011). However, flank slumping and related tsunamis occurred during several recent lava effusions (namely in 1879, 1916, 1919, 1930, 1944 and 1954, according to Barberi et al., 1993). The so-called "major" explosions are intermediate between mild Strombolian explosions and paroxysms: in these cases the ejected material may reach the summit and the surrounding areas, thus being a main thread to hikers.

2.1. Stromboli recent major eruptions

Stromboli reactivated the scientific interest with the onset of the major eruption that started on December 28, 2002, when a lava effusion from the crater area was followed, on December 30, by a composite slump down the northern flank of the cone (named Sciara del Fuoco, a horseshoe-shaped scarp open north-westward) that collapsed into the sea and generated a tsunami: the wave propagated to the main village and affected the north-eastern coast of Sicily causing several damages (Tinti et al., 2006; Baldi et al., 2008). Following this event, a multidisciplinary effort was promoted by Italian Civil Defense authorities to mitigate volcanic risk in this sector of the Mediterranean. In the following days, summit vents were dismissed and the NE sector of the crater terrace collapsed. The lava flow continued from vents located at a lower altitude (~700 m. a.s.l.) until July 2003 with progressively decreasing effusion rates (Calvari et al., 2005; Baldi et al., 2005). A paroxysmal explosion occurred on April 5, 2003 with the ejection of a 1 km high column of ash, pumices, bombs and blocks (Bonaccorso et al., 2003; Calvari et al., 2005; Ripepe et al., 2005). The

geochemical data that preceded the onset of both lava effusion and the paroxysmal explosion were discussed by Carapezza et al. (2004) and Cigolini et al. (2005). The evolution of VLP (very long period) signals, thermal anomalies and SO_2 plume concentrations were analyzed by Ripepe et al. (2005).

The mild strombolian and persisting explosive activity was then resumed by the end of July 2003 (and was accompanied by the progressive ceasing of the lava flow) and continued until February 27, 2007, when the effusion of a new lava flow started at the NE summit vent. In the following days, the original flow ceased and lava effusion continued from a parasitic vent, located at about 400 m above sea level, and continued until April 2, 2007. However, a new and violent paroxysmal explosion occurred on March 15, 2007 with the ejection of ash, pumices, bombs and projectiles that reached some houses of the village of Ginostra. The explosive event was preceded by an anomalous increase in volcanic seismicity that accompanied and followed the nearly vertical collapse of the crater area (Barberi et al., 2009; Neri and Lanzafame, 2009). A moderate seismic and infrasonic activity, characterized by the absence of explosions at the summit vents, persisted until the beginning of July, 2007 when the mild Strombolian activity was finally resumed at the summit vents (namely on Jul 2, 2007). Geochemical data on the above eruptive events were reported by Aiuppa et al. (2009), Rizzo et al. (2009) and Inguaggiato et al. (2011).

The ongoing activity is essentially strombolian but the recorded thermal flux has been increasing since mid 2008 (Coppola et al., 2012). Similarly, major explosions seem to be more frequent when compared to the earlier (pre 2002) eruptive history and occasionally lava overflows may occur (cf., INGV Report 2011-08-02). A geochemical approach to decode precursory signals of major explosions were provided by Aiuppa et al. (2011) and Laiolo et al. (2012).

3. Methods

The methods applied during our radon surveys at Stromboli reflect the evolution of measurement techniques during the last decade. Radon measurements were performed, starting May 2002, by

means of an original network of 25 stations deployed on the NE sector of the cone (Fig. 1b). Following the lava effusion of December 28, 2002 two of these stations were submerged by the flow and, since then, were dismissed. In addition, we removed two other stations that were located onto private property. Thus, the current network consists of 21 measurement sites. Earlier measurements were systematically obtained by exposing track-etch detectors (LR115), finely calibrated for alpha particle beams, and E-PERM® electretes (Kotrappa, 1993). The firsts were exposed from 2 to 5 weeks, whereas the seconds were exposed from one to 4 days during our periodic surveys. In both cases radon activities represent integrated measurements over their exposure time. Detector were placed in capped pipe-like samplers (1.20 m long and a diameter of 12 cm) that were inserted into the soil down to a depth of about 60 cm. Both types of detectors can coexist and they are placed at about 50 cm above the inner soil bottom. The exposure of the above detectors gave us the opportunity to correlate radon emissions with short-and-long period variations in volcanic activity.

Since November 2005 we expanded the network of periodic measurements to cover the whole island by adding 17 new stations for periodic measurements (see Table 1). Since May 2005 we deployed three automatic stations. One was fixed at the summit (the Pizzo station, named PZZ) and two others were placed at lower altitudes and their location was changed throughout 2005 and 2007. In this paper, beside analyzing the data collected at the summit (cf. station 6 in Fig. 1b, 8 and Table 1), we will treat some automatic data collected at station 13 (i.e., along the N60°E fracture zone). In this cases, the radon detector was a DOSEman sensor produced by SARAD Gmbh. It was inserted into a polycarbonate case (permeable to radon) and connected to a solar panel for continuous energy supply. In this cases the sampling time was set every 4 hours and the data were stored into a memory card that was periodically downloaded.

Within a single automatic station, the DOSEman is positioned within a polycarbonate case inserted into PVC box (open downward). This box is set into the soil down to a depth of ~1 m. The box inner volume is occupied by “free soil air” and the gas is passively fluxing into the atmosphere

through a tube placed at the top of the PVC box. This tube is interconnected with an "expansion reservoir" that minimizes the effects of atmospheric changes. The DOSEman electronic dosimeter consists of a measurement chamber (cylindrical in shape and 12 cm^3 in volume membrane) where the charged alpha particles concentrate onto a Si-doped semiconductor detector. Here, they are counted by an automated alpha spectrometer and are stored and processed by a multichannel analyzer that subdivides counts into Regions of Interest (ROIs), and generates the spectrum of the radon gas in terms of energetic domains. The sensitivity of the instrument is comprised between 10 Bq/m^3 to 4 millions of Bq/m^3 (Streil et al., 2002; Gründel and Postendörfer, 2003). DOSEman is recording decays with energy comprised between 4500 and 10000 keV: thus including the peaks of ^{222}Rn plus the peaks of its daughters (^{218}Po and ^{214}Po; at 6200 and 8000 keV, respectively) together with that of ^{220}Rn (thoron, due to the decay of the ^{232}Th chain). The counts for ^{214}Po must be corrected since part of the ^{220}Rn spectrum overlaps the ^{214}Po peak and about 7.5 % of these counts are ascribed to thoron (cf., Gründel and Postendörfer, 2003). Radon concentrations (Bq/m^3) are derived from the ROIs total counts by introducing a calibration factor (C_{f_i}):

$$C_i[Bq/m^3] = (C_{f_i}/Cts * (1/t_s)) * 1000 \quad (1)$$

where *Cts* are the counts, t_s is the sample time (in minutes) and 1000 is the factor for converting kBq/m^3 into Bq/m^3. Radon can be computer in *fast mode* (that includes the counts of both ^{222}Rn and ^{218}Po) as well as in *slow mode* (that takes into account the counts of ^{214}Po, as well) (cf., Gründel and Postendörfer, 2003). We essentially used the fast mode option since ^{214}Po is usually clustering with aerosol particles and we can bypass ^{220}Rn interferences on ^{214}Po peaks. The estimated average error at radon concentration approaching 1000 Bq/m^3 is ± 25%, exponentially decreasing at higher radon activities (Streil et al., 2002).

Staring from April 2007 we deployed two real time stations that are currently operative. Real time measurements will not be further discussed in this paper since they have been treated in earlier contributions (cf., Cigolini et al., 2009; Laiolo et al., 2012).

Geophysical signals on tremor amplitude and infrasonic puffing were recorded as follows. The seismic tremor amplitude is computed as the root-mean-square (RMS) of the seismic (UD component) records using 1-minute-long window. Beside explosive degassing, infrasonic puffing at Stromboli represents the ‘‘overpressurized’’ and a ‘‘discrete’’ counterpart of the continuous and passive degassing of the magma column (cf., Ripepe et al., 2007; Harris and Ripepe, 2007). Infrasonic puffing amplitude is here computed as the 1-minute-long average of the pressure detected by mean of a small-aperture infrasonic array (Ripepe et al 2007). At Stromboli, tremor and infrasonic amplitudes are normally well-correlated, indicating a common source whose dynamics reflect degassing processes affecting the magma column. Changes of seismic tremor and infrasonic puffing amplitudes observed in our dataset, hence, can be related to fluctuations in degassing regimes within an active magma column (Falsaperla et al., 1994; Ripepe and Gordev, 1999; Harris and Ripepe, 2007).

4. Periodic measurements and radon mapping

We started our radon survey in May 2002. Originally, we planned to measure monthly seasonal variations in radon emissions and relate them to long term changes in volcanic activity. During our monthly surveys we restricted our analysis on short-term changes by exposing E-PERM® electretes. The cross-check of the data acquired by these two methods has been particularly helpful in analyzing the onset and evolution of the 2002-2003 eruptive sequence. Our data indicated that both the onset of the effusive eruption (on December 28, 2002) and the paroxysmal explosion of April 5, 2003 were preceded by radon emissions higher than 20,000 Bq/m^3 at three of the summit stations (Cigolini et al., 2005). These type of measurements continued until the end of 2007. By that time we have collected about 2,600 radon measurements by E-PERM® electretes and over 1,400 data by

using LR115. Data obtained by using LR115 allowed us to draw a timeseries of the monthly average ^{222}Rn emissions on the entire radon network (cf. Cigolini et al., 2009). Moreover, we were able to retrieve background, threshold and anomaly values for all the stations of the network by means of E-PERM® measurements. These parameters were obtained according to the graphical method of Sinclair (1974), recently used in several geochemical studies (e.g., Hernandez et al., 2004; Carapezza et al., 2009; Padrón et al., 2013). In Fig. 2 we report the data analyzed at three selected stations (all other values are reported in Appendix A). On a whole, acquired data show mean ^{222}Rn concentrations comprised between 2,000 and 5,000 Bq/m^3, with the exception of few sites that show average values higher than 20,000 Bq/m^3 (cf. St6 and St10 in Fig. 1b). The firsts of the above are in good agreement with mean concentrations measured at other active volcanoes (Table 2 and references therein).

To be able to visualize radon concentrations in space and time, we are reporting selected maps that "photograph" radon emissions during specific spans of times that are essentially correlated with changes in volcanic activity. Radon concentration maps are constructed onto DEM topographic images: we summarize the isoemissive curves of radon concentrations (identified by variable colours) from the measured concentrations (obtained from E-PERM® detectors). The geometry of the isoemissive curves are calculated by applying the kriging method (e.g., Buttafuoco et al., 2007).

4.1. Radon mapping of the Stromboli Island

In order to have a better picture on how radon is released on the whole island, we integrated our earlier network with 17 new measurement sites, thus covering most of the accessible areas on Stromboli. We were able to expand the original network only on November 2005. Periodic measurements were thus performed from November 2005 to September 2006, and average data (of five measurements for each single station) are reported in Fig. 3. As observed in previous studies (Cigolini et al., 2005; 2009), higher emissions persist in the summit area and along the upper eastern sector (cf. Station 13 in Fig. 1b). Moderately high emissions are also recorded at the NW

edge of the Sciara del Fuoco (Punta dei Corvi), where they reach 10,000 Bq/m^3. All other stations show moderate (up to 5,000 Bq/m^3) and relatively low radon emissions (900-3,000 Bq/m^3). The acquired data define a clear difference between the western and the eastern sector of the summit area. In particular, the latter one (that includes station 13) is related to the N60°E fracture zone characterized by high CO_2 fluxes (cf. Finizola et al., 2002; Carapezza et al., 2009). In a similar fashion, low radon concentrations collected in the western summit sector substantially match the area with lower CO_2 emissions (identified by Finizola et al., 2003). During our periodic surveys we essentially concentrated our data collection on the eastern sector (cf., Cigolini et al., 2005; 2007; 2009).

4.2. Radon mapping during Strombolian Activity: 2002-2007

The display and the collection of the representative data set onto the northeastern sector of Stromboli can be obtained in four hours within two working days, thus minimizing the exposure of the researchers within the summit area (that can be surveyed in about an hour). Here, we report a selection of our data. In this cases, constructed maps summarize the isoemissive curves for radon concentrations together with those obtained from the difference of reference threshold values (obtained by statistical analyses on E-PERM® data for all the stations of the network; Table A1.1) from the measured concentrations.

In Fig. 4a we report the data collected during 21-30 October, 2002 (cf. Cigolini et al., 2005 as well). It can be seen that higher radon concentrations are essentially concentrated around the summit area, involving some stations located on the eastern flank (which are above threshold reference values). Most of the other measurements sites are below the cited values. This is basically consistent with the fact that volcanic activity was moderately increasing (Federico et al., 2008; Coppola et al., 2012). The data collected after the onset of the effusive eruption (December 28, 2002) are reported and described in the following section.

On 9-16 September 2005, radon emissions are radon emissions are low and at only two summit stations radon activities reach 15,000 Bq/m^3 (Fig. 4b) but are still below their reference threshold values. Similarly, only two of the lower stations, located on the eastern flank, show emissions above their relative thresholds. All the others are well below. This arrangement is typical of mild Strombolian activity and indicates that diffuse degassing is moderate.

The overall data collected during 11-16 February 2007 show that ^{222}Rn activities at three summit stations reach values higher than 20,000 Bq/m^3 and well above threshold reference values (Fig. 4c). In addition, the rest of measurements are all below their relative thresholds thus indicating that radon degassing is essentially concentrated at the summit area. As we will discuss in more details later, the onset of the eruption has been also monitored by means of the automatic station located at the summit (station 6, also named PZZ).

4.3. Radon mapping during lava effusions : 2002-3003 and 2007

In Fig. 5a we report the data collected from February 11 to February 16, 2003. It can be see that radon emissions are still high at some summit stations but several others, including few stations at the northern edge of the cone and along the NE ridge of Sciara del Fuoco, show values above reference threshold values. This configuration is due to the fact that during the effusive eruption the fracture network was affected by the adjustment of the volcano edifice, and average effusion rates were still moderate (approaching 0.5 m^3/sec according to Calvari et al., 2005; Harris et al., 2005). It is significant to recall that during January-February 2003 we measured extremely high radon activities along the fractures that were rimming the SW crater (these will be presented in a later section). The most striking result of this scenario is the persisting anomalies at the northern edge of the cone (that involves station 1 and stations 2, see Fig. 1b) that is likely a residual effect inherited from the slumping of the submerged part of the Sciara del Fuoco, occurred on December 30, 2002 just below the western rim of Punta Labronzo (e.g., Baldi et al. 2005; Cigolini et al., 2005; Tinti et al. 2006; Chiocci et al., 2008). In addition, the rest of measurements are all below their relative

thresholds thus indicating that radon degassing is essentially concentrated at the summit area. Here, we then report and discuss the bulk data collected from March 21 to March 26, 2003 (Fig. 5b) that preceded the paroxysmal explosion of April 5 of the same year. During this period high radon concentrations still persist within the summit area and still cover and extended zone onto the eastern sector of the cone. This is also clear when we check the "threshold map", where measured values are well above the reference threshold values. In this case, relatively higher emissions (above their thresholds) are still persisting at the northern edge of the volcano (i.e., nearby Punta Labronzo: station 2; see Fig. 1b).

Finally, we report the data collected from March 10 to March 18, 2007 (Fig. 5c) that overlap the onset of the paroxysmal explosion of March 15. It can be seen that the stations located on the summit as well as two of those positioned along the N60°E fracture zone (station 13 and 15 in Fig. 1b) are well above threshold reference concentrations. A similar setting is also reported at the stations at the northern edge. The whole scenario is consistent with anomalous degassing related to the opening of the fracture network during the ongoing eruption.

5. Automatic radon measurements: 2005-2007

Automatic measurements started on May 26, 2005. Data are reported in Fig. 6 together with local environmental parameters. It can be seen that the radon peak of June 2005 (slightly above 20,000 Bq/m3) is decoupled from environmental parameters and, therefore, is essentially related to summit degassing. Then, radon decreases reaching 6,000 Bq/m3 just prior the major explosion of August 5 of that year. In the following days, radon emissions increase and moderately fluctuate during a decreasing trend in local temperatures. During late November-early December 2005 there is an increasing trend in radon concentrations coeval with marked decreasing trends both in temperature and atmospheric pressures associated with moderate, but continuous, rain fall conditions (cf., Fig. 6d). Then, radon activities sharply decrease by the end of January-February 2006. This period (from June to 2005 to February 2006) was characterized by the typically mild Strombolian activity. Since

then the radon signal amply fluctuate between March and April 2006. This feature is essentially coeval with the onset of a vigorous strombolian activity at summit vents (see Fig. 6a). During this periods atmospheric parameters sharply fluctuate and pressure reaches its minimum by March 15 (accompanied by rain fall), being decoupled from the radon peak (up to 22,000 Bq/m^3). Interesting correlations are revealed by plotting radon data with those of other geophysical parameters, such as tremor amplitude and infrasonic puffing (Fig. 7).

On a monthly scale, in fact, the increase in strombolian activity is also evidenced by a drastic increase of infrasonic puffing and tremor amplitude ~2-3 times average values, thus reaching 6 Pa and 5 μm/s, respectively. This phase of increased activity ends with a seismic sequence of 3 volcano-tectonic earthquakes (Apr, 18, May 5 and 6, 2006, M_D 3.2 3.4 and 2.3, respectively; light grey area in Figure 7) located at a shallow depth within the edifice (D'Auria et al., 2006). Radon activity peaked at 24,000 Bq/m^3 and preceded the onset of the earlier quake. After these events radon emissions and volcanic activity decrease and stabilize until December 2006. Tremor amplitude fell to the mean levels ~2 μm/s. but infrasonic activity was still higher than the earlier one (prior December 2005). Similarly, radon activities seem to be unaffected by the decreasing trend in temperatures, changes in atmospheric pressure and rain falls (Fig. 6). This is likely due to the fact fluid motion, at summit stations, is essentially dominated by fluid advection.

At the beginning of January 2007 there was only a slight increase in radon concentrations that, in turn, drastically increased on February 19 and peak to 23,500 Bq/m3, one day before the onset of the effusive eruption of February 27, 2007. Similarly, the trend of infrasonic puffing and seismic tremor show a clear increase since January 2007 and persist on very-high level during February 2007 (cf., Ripepe et al., 2009). Very high radon activity persist until March 2 and then decrease to lower values whereas the signal of the infrasonic puffing was absent and seismic tremor dropped to very low values **(**Fig. 7b-c). This is substantially coeval with the opening of a new effusive fissure at the base of NE crater that marks the ceasing of the typical Strombolian activity at summit vents

(Aiuppa et al., 2009; Ripepe et al., 2009). Following this event tremor amplitude decrease and infrasonic puffing dropped to zero. Since then the summit craters were dismissed and the lava effusion was taking place from a fissure vent located at ~400 m a.s.l. (Neri and Lanzafame, 2009).

6. Extremely and very high Radon Emissions

In this section we present some of the collected data characterized by extremely and very high radon activities. Some of these data were collected along a main fracture that was rimming the SW crater during January and February 2003 (cf. Fig. 8a,c and Table 3). It must be recalled that during this span of time radon concentrations were particularly higher at most of the stations of the network (see above) due to the fact that the volcanic edifice, during to the ongoing effusive eruption, was still under adjustment. Luckily, volcanic activity at summit craters was dismissed, and the lava was effusing from a vent located nearby the eastern scarp of Sciara del Fuoco (at an altitude of about 710 m a.s.l.). Three sites of measurements were selected along the cited fracture at about 100 m from each other so that the monitored front was about 300 m in length. In addition, we collected some data on the eastern edge of Sciara del Fuoco, at a site named Bastimento (740 m a.s.l., cf. Fig. 8b), where some fumaroles activated (during the second week of February) along a fracture zone representing the northeastern propagation of craters' alignment (striking N40°E). Moreover, during the 2002-2003 effusion this sector was affected by an intense NW-SE fracturing due to the syneruptive propagation (toward the north) of the NE-SW eruptive fissure (Acocella et al., 2006). A summary of data are reported in Table 3. It can be seen that, on January 14 average radon concentration along the SW crater rim (see Fig. 8c) reached values of about 525,650 Bq/m^3, with one of the site boosting to 1,479,607 Bq/m^3. The next day average activities are just slightly above 115,000 Bq/m^3. Average measurements performed on February 9 are still approaching 485,900 Bq/m^3, with one of the sites reaching 1,397,000 Bq/m^3. Three days later, emissions are still high and average 606,000 Bq/m^3, with the above site up to about 1,592,000 Bq/m^3. Notably, Finizola and coauthors (2009) reported that during January, 2003 this sector was characterized by

higher values in soil temperature and CO2 concentration (up to 90°C and 800,000 ppm; respectively).

Measurements along the eastern propagation of the craters alignment (Bastimento) were performed on February 11, 12 and 13 (sites were located at about 10 m distance). In this cases average values are well below the ones collected at the crater rim, and are comprised between 86,500 and 417,326 Bq/m^3 with one of the sites peaking to 754,742 Bq/m^3. During March 2003 there was an increase of Strombolian activity recorded with the occurrence of some explosive events at the summit central crater that projected blocks several hundreds meters from the crater area, thus increasing the hazard for researchers operating within the surroundings. For these reasons systematic measurements on the above sites ceased.

However, we also detected some extremely high radon concentrations during our automatic measurements. A very interesting scenario occurs during June 2007. At that time, besides monitoring the summit station (PZZ, Fig. 9a), we displayed an automatic detector at station 13 (Fig. 9b). During this period Strombolian explosions were rare and volcanic activity was characterized by degassing at the active vents coupled with mild ash emissions. In addition, there was an upward migration of the VLP source associated with a drastic increase in soil temperature within the summit area (cf. Rizzo et al., 2009). During early and mid-June, the summit station was recording a rather stable radon signal in the range of 10,000 (± 1,000) Bq/m^3. In the late morning of June 20 it first increased above 20,000 Bq/m3 and by the evening of that day it peaked up to about 37,500 Bq/m^3. In the next few hours it progressively decreased (down to about 7,000 Bq/m^3) and on June 21 there was a second minor peak up to 27,393 Bq/m^3. For the next two days the signal was relatively stable fluctuating from 7,400 to about 6,000 Bq/m^3. This sequence was a prelude to the boosting of the radon signal on June 23, that reached a value of 472,063 Bq/m^3, and was followed by two double peaks during the next two days (142,854 and 180,542 Bq/m^3 on June 24 and 25, respectively). In between, radon activities were down to about 10,000 Bq/m^3. A similar pulsating signal occurred on June 26 (440,188 Bq/m^3) and June 27 (167,958 Bq/m^3) (Fig. 9a).

Conversely, station 13 has been constantly decreasing during early and mid-June. In fact, from initial values of ~ 12,000 Bq/m^3 radon emissions reach near-minima values of about 300 Bq/m^3 on June 20, 2007. In the next days radon concentrations are persistently very low, and below 100 Bq/m^3, likely due to the fact that gaseous transfer along this facture has been dismissed and/or the fracture has been temporarily sealed (Fig. 9b).

We think that the above sequence it photographs the dynamic response of the two fractures so that while one is reactivated the other is dismissed and sealed. It is therefore likely that similar processes occur so within the volcano edifice and fluid transport is strongly controlled by the fracture network.

Intriguing questions arise if we consider analyse the data for thoron as well (Fig. 10). It can be seen that the two signals are essentially concordant and both reach extremely high values. This is likely related to the fact that fracturing involved the near-surface rocks during degassing as well. However, since both ^{222}Rn and ^{220}Rn have concordant peaks it is likely that the fracturing that led to radon anomalies were somehow deeper and likely involved a strongly advective component, which is not unusual in this environment. Therefore, our monitoring system recorded the effects of these two processes associated with fracturing events that originated at depth and propagated to the surface. This process was characterized by pulsating episodes that started twelve days before the reactivation of the typical strombolian activity at summit vents (i.e., on Jul 2, 2007).

To be able to set some geological constraints in the light of the above data, we performed some estimates on the possible depth of the fractures that affect the summit area. Fumarolic gases in this sector are water dominated with XCO_2 fractions ranging from 0.07 to 0.10 (Finizola et al., 2003). Geothermometric estimates on these gases, following Chiodini and Cioni (1989), give equilibration temperatures of 260-275°C (and will be called low temperature, LT fluids). However, gases sampled by Maurizio Ripepe along the fractures surrounding the active craters are CO_2 richer, with XCO_2 reaching 0.67 and a sampling temperature of 410°C (Martini et al., 1996). This CO_2 fraction is very similar to the ones measured in melt inclusions (e.g., Bertagnini et al., 2003; Metrich et al.,

2010). Thus this type of fluids will be called high temperature, HT fluids). Since their rise is strongly dominated by convection/advection, we used the set of equations of Lapwood (1948) and Cathles (1997) recently summarized by Cigolini (2010) to estimate a possible depth for the feeding fractures (see Appendix B). In doing so we have to force the radon-bearing fluid to reach the surface within 4 hours (i.e., the average time span for the onset of the radon spikes reported in Fig. 10a, which the sampling time of our detector). By substituting the proper rock and fluid parameters, the depths of the fractures that feed gaseous release at Stromboli summit are constrained to 200 m (for LT fluids) and 310 m (for supercritical CO_2 rich HT fluids of the crater rim). However, under dynamic conditions these gas-filled fractures easily propagate up to the surface. Here is where the peaks of thoron occur, being essentially related to near-surface fracturing of surface rocks associated with the occurrence of diffusive processes. According to Giammanco et al. (2007) thoron anomalies are mainly related to surface cracking that affect the porous medium at depths of about 6 m at the most.

7. Discussion and conclusions

Although open conduit volcanoes may show very low radon emissions in proximal and distal areas since gas is mainly concentrated within the plume itself (Williams-Jones et al., 2000; Varley and Armienta, 2001), the mapping of radon at Stromboli volcano show localized zones of diffuse degassing. These are mainly concentrated along major fractures and/or above sectors affected by hydrothermal activity. Statistical analyses show that emissions above threshold reference values generally occur before and/or during effusive phases. This is due to the opening of the fracture network and concurrent structural adjustment of the cone. Earthquake-volcano interactions were also recorded and showed preseismic, coseismic and post-seismic radon anomalies at the above sites (e.g., Cigolini et al., 2007). Nevertheless, precursory signals of effusive-explosive phases are essentially recorded at summit stations.

Trends in radon concentrations may be compared with other geophysical parameters and give us the opportunity to better understand the changes in volcanic activity. In this frame, the 2005-2007 radon time series is somehow correlated with variations in infrasonic and seismic tremor amplitudes. However, the radon signal is more disturbed and, in some cases, it may be decoupled from seismic tremor but they both reach their relative maxima within a period of vigorous Strombolian activity. At Stromboli, seismic tremor amplitude is usually correlated with the level of explosive activity (Falsaperla et al., 1998). Seismic data indicate that its source is confined within the magma column at relatively shallow depths (< 300 m) (Chouet et al., 1997). Moreover, seismic tremor and infrasonic puffing seem to have a common source likely related to in-conduit degassing (Harris and Ripepe, 2007; Ripepe and Gordev, 1999).

Refilling of volatile-rich magma is invoked to explain periods of increasing Strombolian activity with high tremor levels and high explosive regimes (Falsaperla et al., 1998), generally coupled with increasing degassing (Carapezza et al., 2004; Cigolini et al., 2005). The March-May 2006 and January-February 2007 phases, characterized by high radon concentrations, infrasonic and seismic tremor amplitude (cf. Fig. 7), represent two of such refilling episodes. The first is characterized by an unusual volcano-tectonic activity likely associated with the fracturing of the upper part of the reservoir due to magma ascent. The second precedes the onset of the February 2007 lava eruption. In our view, these processes represent two different mechanisms for dissipating magma overpressures within the shallow feeding system.

An additional issue is the one dealing with extremely high radon emissions recorded at Stromboli. Such extremely high values are not unusual on active volcanoes: at Mount Etna, Neri et al. (2006) recorded average radon activities above 10^6 Bq/m^3, with peak values reaching 1.7 x 10^8 Bq/m^3. The firsts were recorded during effusive and Strombolian activity (from July 15 to July 24, 2006), whereas peaks values were reached during the opening of a new vent (at the base of the SE summit crater) with associated Strombolian explosions and lava fountaining (July 19, 2006). However, extremely high concentrations are not unusual in nature. Nikolopoulos et al. (2012) found radon

emissions reaching 500,000 Bq/m^3 during a very seismically active period occurred in South West Greece. Moreover, Žunić et al. (2006) detected peaks of about 2,000,000 Bq/m3 in a thermal area of the Balkan region. Gillmore et al. (2001) reported some extreme concentrations up to 7,100,000 Bq/m^3 in the abandoned metalliferous Bushdown mine (Devon, Southwest England). Here, granitic rocks intrude a Devonian-Carboniferous sequence consisting of slates, shales, sandstones and limestones.

As previously discussed, extremely high radon emissions at Stromboli were recorded in February-March 2003 and seem to be connected with the opening of the fracture network in the area surrounding the craters. These anomalous radon concentrations were likely associated with the structural adjustment of the summit area that followed the onset of the effusive activity and the implosion of the NE and central craters. A similar scenario also occurs during the ongoing eruption of 2007.

Automatic measurements with extreme radon concentrations (collected in late June- early July 2007) give us the opportunity to estimate the relative depths of the fractures nearby the summit ridge (named Pizzo where LT fluids are released) and those that surrounds the summit craters (HT fluids). Our estimates suggest that their depths are constrained between 200 and 310 m, respectively. This is in good agreement with the recent findings of Longobardi et al. (2012) who localized the hypocentral depths of the so called "hybrid events" at similar depths during the early stages of the 2007 effusive phase. In addition, the above depths are consistent with the source of the very long period seismic signals (VLP) localized at a depth of about 500 m a.s.l. below the upper-central part of the Sciara del Fuoco (Chouet et al., 1997, Marchetti and Ripepe, 2005). However, fracturing associated with vigorous degassing may contribute to trigger slope instability, particularly during dike injections that precede the onset of major effusive events.

It significant to emphasize that the extremely high radon emissions were recorded during (2003) or after the end (2007) of effusive phases, and, in both cases, before the reactivation of strombolian activity at the summit craters (that imploded and were dismissed after the onset of both effusive

phases). This indicate that magma ascent is accompanied by the progressive fracturing of the wallrocks. Radon data collected by automatic measurements also suggest that this process occurs with a sequence of pulsating degassing episodes associated with fluid motion toward the surface.

Finally, we have shown that measuring radon at open-system volcanoes throws light on the dynamics of degassing processes and their evolution in space and time. Therefore, radon monitoring is not only a precious tool to detect precursory signals of volcanic eruptions but is also an additional method to investigate transitions in volcanic activity during changing eruptive scenarios.

Acknowledgments. This research has benefited from funding provided by the Italian Presidenza del Consiglio dei Ministri - Dipartimento della Protezione Civile (DPC). Scientific papers funded by DPC do not represent its official opinion and policies. This work is part of the Cooperative Project between the Departments of the Earth Sciences of the University of Florence and the University of Turin. The manuscript has been greatly improved by the critical comments and suggestions of M. Neri and an anonymous reviewer.

APPENDIX A

Summary of the location of the stations of the Stromboli radon network that are opportunely georeferred (Table A1). The Table also reports single background, threshold and anomaly values, obtained following the graphical method of Sinclair (1974) recently applied by several authors (e.g., Hernandez et al., 2004; Carapezza et al., 2009; Padrón et al., 2013). Measurements were performed by using EPERM® electretes.

APPENDIX B

To constrain the depth of the fractures that feed fumarolic (LT) and supercritical (HT) fluids that respectively reach the summit area (named Pizzo) and the craters' rims, we introduce the following relationship for fluid advection-convection within a porous medium (Lapwood, 1948)

$$kgH^2\left(\frac{dT}{dz}\right)\left(\frac{d\rho_f}{dT}\right) = R_a D_m \eta \qquad (1)$$

where k, g and H are the permeability, the acceleration of gravity and the height of the convective cell, respectively. The term dT/dz is the temperature gradient whereas $d\rho_f/dT$ is the differential of the fluid density in respect to temperature. R_a is the Rayleigh number, D_m is the thermal diffusivity of the fluid filled medium, and η is the viscosity of the fluid. Fluid convection within a porous medium is ruled by the condition $R_a > 4\pi^2$. The thermal diffusivity is related to the rock thermal conductivity K, density ρ_m, and C_m specific heat of the porous medium according to: $D_m = K/\rho_m C_m$. By introducing the fluid thermal expansion α, and the local geothermal gradient $G_T = dT/dz$, we may solve equation (1) for the Rayleigh number

$$R_a = C_m \rho_m k \rho_f \alpha g H^2 G_T / \eta K \quad (2)$$

The maximum vertical flow rate (or Darcy's velocity) within a confined porous medium can be approximated by (Cathles, 1997; Cigolini, 2010),

$$J_z \approx \sqrt{2} K (R_a - 4\pi^2)^{1/2} / \rho_f C_f H \quad (3)$$

where C_f is the fluid specific heat.

Since fluid motion is controlled by porosity, ϕ, the true velocity of the pore fluid is $v_f = J_z/\phi$. In our calculations we first considered a water dominated fluid with XCO_2 of 0.90 and an equilibration temperature of 270°C, typical of the fumaroles of the summit (Finizola et al., 2003). Secondly, we considered a supercritical fluid with XCO_2 of 0.67 and T=410°C sampled in the fractures surrounding the NE crater (see text for references). As previously mentioned, our goal is to estimate the possible depths of the factures associated with extremely high radon emissions. We therefore assume the carrier gases (water and carbon dioxide mixtures) will follow an adiabatic decompression and finally cool, due to their expansion within the last few meters (before reaching the atmosphere; e.g., Chiodini and Marini, 1998; Cigolini, 2010).

However, the choice of the appropriate physical parameters are critical for estimating reliable depths. Among these, the geothermal gradient has considered to approach 160 °C/km (being consistent with the temperature distribution of Gervino et al., 2004; and the equilibration depth of

6.5 km obtained on gabbroic nodules that surround the magma chamber at ~1030°C). In addition, the permeability (k) of the summit lava-bearing pyroclastic sequence was set at 10^{-12} m^2, being consistent with Freeze and Cherry (1979) and Cigolini et al. (2001). Similarly, the absolute porosity (ϕ) along fractures zones was first considered in the range of 10^{-4} and 10^{-5} (cf. Ventura and Vilardo, 1999; Cigolini, 2010). Another critical parameter is thermal conductivity (K): we have chosen a value of 2 Wm/K for the sequence of the summit (Pizzo section, dominated by ± altered pyroclastic rocks; e.g., Rosi et al., 2000) with bulk density ρ_m about 1800 kg/m^3, and a value of 2.8 Wm/K for the sequence surrounding the active crater where the rocks are more massive and continuous (due to dike injection) with a bulk density of 2600 kg/m^3 (cf., Robertson and Peck, 1969; Clauser and Huenges, 1995). The specific heat of the fluid-filled medium is considered 10^3 J/kg*K (e.g., Cathles, 1997).

Densities and thermal expansion for the above fluid mixtures were calculated by using the Modified Redlich Kwong equation of Holloway (1977), whereas fluid viscosities and the specific heats of fluids were calculated, assuming ideal mixing, from the data of Lemmon et al. (2005) available at http://webbook.nist.gov.

Input data are summarized in Table B.1 together with our best estimates for the heights of the convective cells. These were obtained by forcing the fluid to reach the surface within 4 hours (i.e., 0.167 days which the sampling time of our detector and represents the maximum time for the fluid to reach the surface to give the observed ^{222}Rn spikes, see Fig. 9a and 10a). Thus our best estimates for H are 195 m and 310 m, for low temperature fluids and high temperature fluids, respectively. To get plausible results, consistent with the geometry of the fracture network, we have to constrain porosities at 10^{-4} (since lower values will lead to unrealistically high H values and do not satisfy the previously set time-related constraints).

References

Acocella, V., Neri, M., Scarlato, P., 2006. Understanding shallow magma emplacement at volcanoes: Orthogonal feeder dikes during the 2002-2003 Stromboli (Italy) eruption, Geophysical Research Letters 33, L17310. doi:10.1029/2006GL026862.

Acocella, V., Neri, M., 2009. Dike propagation in volcanic edifices: Overview and possible developments. Tectonophys 471(1–2), 67-77.

Aiuppa, A., Federico, C., Giudice, G., Giuffrida, G., Guida, R., Gurrieri, S., Liuzzo, M., Moretti, R., Papale, P., 2009. The 2007 eruption of Stromboli volcano: Insights from real-time measurement of the volcanic gas plume CO_2/SO_2 ratio. Journal of Volcanology and Geothermal Research 182(3–4), 221-230.

Aiuppa, A., Burton, M., Allard, P., Caltabiano, T., Giudice, G., Gurrieri, S., Liuzzo, M., Salerno, G. 2011. First observational evidence for the CO_2-driven origin of Stromboli's major explosions. Solid Earth 2, 135–142. doi:10 5194/se-2-135-2011.

Alparone, S., Behncke, B. , Giammanco, S., Neri, M., Privitera, E., 2005. Paroxysmal summit activity at Mt. Etna (Italy) monitored through continuous soil radon measurement. Geoph. Res. Lett. 2, L16307. doi:10.1029/2005GL023352.

Baldi, P., Fabris, M., Marsella, M., Monticelli, R., 2005. Monitoring the morphological evolution of the Sciara del Fuoco during the 2002-2003 Stromboli eruption using multi-temporal photogrammetry. ISPRS J. Photogramm. Rem. Sens. 59(4), 199-211.

Baldi, P., Coltelli, M., Fabris, M., Marsella, M., Tommasi, P. 2008. High precision photogrammetry for monitoring the evolution of the NW flank of Stromboli volcano during and after the 2002–2003 eruption. Bull. Volcanol. 70, 703–715.

Barberi, F., Rosi, M., Sodi, A., 1993. Volcanic hazard assessment at Stromboli based on review of historical data. Acta Vulcanol. 3, 173-187.

Barberi, F., Civetta, L., Rosi, M., Scandone, R., 2009. Chronology of the 2007 eruption of Stromboli and the activity of the Scientific Synthesis Group. J. Volcanol. Geotherm. Res. 182(3-4), 123-130.

Blackburn, E.A., Wilson, L., Sparks, R.S.J. 1976. Mechanics and dynamics of strombolian activity. J Geol Soc Lond 1 32, 429-440.

Bertagnini, A., Métrich, N., Landi, P., Rosi., M. 2003. Stromboli volcano (Aeolian Archipelago, Italy): An open window on the deep-feeding system of a steady state basaltic volcano. J. Geophys. Res. 108-7, 1-15.

Bonaccorso, A., Calvari, S., Garfy, G., Lodato, L., Patane, D., 2003. Dynamics of the December 2002 flank failure and tsunami at Stromboli volcano inferred by volcanological and geophysical observations. Geophys. Res. Lett. 30-18, 1941. doi:10 1029/2003GL017702.

Bonforte, A., Federico, C., Giammanco, S., Guglielmino, F., Liuzzo, M., Neri, M., 2013. Soil gases and SAR data reveal hidden faults on the sliding flank of Mt. Etna (Italy). Journal of Volcanology and Geothermal Research 251, 27–40. doi:10.1016/j.jvolgeores.2012.08.010.

Burton, M., Neri, M., Condarelli, D., 2004. High spatial resolution radon measurements reveal hidden active faults on Mt. Etna. Geoph. Res. Lett. 31, L07618.

Buttafuoco, G., Tallarico, A., Falcone, G., 2007. Mapping Soil Gas Radon Concentration: A Comparative Study of Geostatistical Methods. Environ. Monit. Assess. 131(1-3), 135-151.

Calvari, S., Spampinato, L., Lodato., S., Harris, A.J., Patrick, M.R., Dehn, J., Burton, M., Andronico, D., 2005. Chronology and complex volcanic processes during the 2002-2003 flank eruption at Stromboli volcano (Italy) reconstructed from direct observations and surveys with a handheld thermal camera. J. Geophys. Res. 110, B02201. doi:10.1029/2004JB003129.

Carapezza, M.L., Inguaggiato, S., Brusca, L., Longo, M., 2004. Geochemical precursors of Stromboli 2002–2003 eruptive events. Geophys. Res. Lett. 31-7. doi:10.1029/2004GL019614.

Carapezza, M.L., Ricci, T., Ranaldi, M., Tarchini, L. 2009. Active degassing structures of Stromboli and variations in diffuse CO_2 output related to the volcanic activity. J. Volcanol. Geotherm. Res. 182 (3-4), 231-245.

Cartagena, R., Olmos, R., López, D.L., Soriano, T., Barabona, F., Hernández, P.A., Pérez, N.M., 2004. Diffuse soil degassing of carbon dioxide, radon and mercury at San Miguel volcano, El Salvador. In: Rose W.I., Bommer J.J. Lopez D.L., Carr M.J. and Major J.J. (Eds), Natural Hazards in El Salvador: Boulder, Colorado, Geological Society of America Special Paper, 375, 203-212.

Cathles, L.M. 1997. Thermal aspects of ore formation. In: Barnes HL (Eds) Geochemistry of hydrothermal ore deposits. Wiley, New York, pp 191–227.

Chiocci, F.L., Romagnoli, C., Tommasi, P., Bosman, A. 2008. The Stromboli 2002 tsunamigenic submarine slide: Characteristics and possible failure mechanisms. Journal of Geophysical Research B: Solid Earth 113 (10) , art. no. B10102.

Chiodini, G., Cioni, R., 1989. Gas barometry for hydrothermal systems and its application to some Italian geothermal areas. Appl. Geochem. 4, 465-472.

Chiodini, G., Marini, L., 1998. Hydrothermal gas equilibria: The H2O-H2-CO2-CO-CH4 system. Geochim Cosmochim Acta 62(15), 2673-2687. doi: 10.1016/S0016-7037(98)00181-1.

Chirkov, A.M. 1975. Radon as a possible criterion for predicting eruptions as observed at Karymsky volcano. Bull. Volcanol. 39, 126-131.

Chouet, B., Saccorotti, G., Martini, M., Dawson, P., De Luca, G., Milana, G., Scarpa, R., 1997. Source and path effects in the wavefields of tremor and explosions at Stromboli Volcano, Italy. J. Geophys. Res. 102, 15,129–15,150.

Cigolini, C., 2010. The dynamics of a double-cell hydrothermal system in triggering seismicity at Somma-Vesuvius: Results from a high-resolution radon survey. Bull. Volcanol. 72-6, 693-704.

Cigolini, C., Salierno, G., Gervino, G., Bergese, P., Marino, C., Russo, M., Prati, P., Ariola, V., Bonetti, R., Begnini, S., 2001. High-resolution Radon Monitoring and Hydrodynamics at Mount Vesuvius. Geoph. Res. Lett. 28 (21), 4035-4039.

Cigolini C., Gervino, G., Bonetti, R., Conte, F., Laiolo, M., Coppola, D., Manzoni, A. , 2005. Tracking precursors and degassing by radon monitoring during major eruptions at Stromboli Volcano (Aeolian Islands, Italy), Geophys. Res. Lett. 32, L12308. doi:10.1029/2005GL022606.

Cigolini, C., Laiolo, M., Coppola, D., 2007. Earthquake-volcano interactions detected from radon degassing at Stromboli (Italy). Earth Planet. Sci. Lett. 257, 511-525.

Cigolini, C., Poggi, P., Ripepe, M., Laiolo, M., Ciamberlini, C., Delle Donne, D., Ulivieri, G., Coppola, D., Lacanna, G., Marchetti, E., Piscopo, D., Genco, R., 2009. Radon surveys and real-time monitoring at Stromboli volcano: influence of soil temperature, atmospheric pressure and tidal forces on ^{222}Rn degassing. J. Volcanol. Geotherm. Res. 184(3-4), 381-388.

Cigolini, C., Laiolo, M., Coppola, D., Ulivieri, G., 2013. Preliminary radon measurements at Villarrica volcano, Chile. J. South Americ. Earth Sci.. doi: 10.1016/j.jsames.2013.04.003.

Clauser, C., Huengens, E., 1995. Thermal conductivity of rocks and minerals. In: Ahrens, TJ (Eds) Rock Physics and Phase Relations-a Handbook of Physical Constants, AGU Reference Shelf 3, pp.105-126, American Geophysical Union, Washington.

Connors, C., Hill, B., La Femina, P., Navarro, M., Conway, M., 1996. Soil Rn-222 pulse during the initial phase of the June August 1995 eruption of Cerro Negro, Nicaragua. J. Volcanol. Geothermal Res. 73, 119-127.

Coppola, D., Piscopo, D., Laiolo, M., Cigolini, C., Delle Donne, D., Ripepe, M., 2012. Radiative heat power at Stromboli volcano during 2000–2011: Twelve years of MODIS observations. J. Volcanol. Geotherm. Res. 215-216, 48-60.

Cox, M.E., 1980. Ground Radon Survey of a Geothermal area in Hawaii. Geoph. Res. Lett. 7, 283-286.

Cox, M.E., 1983. Summit outgassing as indicated by Radon, Mercury and pH mapping, Kilauea Volcano, Hawaii. J. Volcanol. Geotherm. Res. 16, 131-151.

D'Auria, L., Giudicepietro, F., Martini, M., Orazi, M., 2006. The April–May 2006 volcano-tectonic events at Stromboli volcano (Southern Italy) and their relation with the magmatic system. Earth-Prints open archives. http://www earth-prints org/handle/2122/1506.

De Astis, G., Ventura, G., Vilardo, G., 2003. Geodynamic significance of the Aeolian volcanism (Southern Tyrrhenian Sea, Italy) in light of structural, seismological, and geochemical data. Tectonics 22/4, 1040/14.

Duenas Fernández,, M.C., Carretero, J., Liger, E., Pérez, M., 1997. Release of ^{222}Rn from some soils. Ann. Geophysicae 15, 124-133.

Falsaperla, S., Montalto, A., Spampinato, S., 1994. Seismic investigations on volcanic tremor at Stromboli volcano (Italy). Acta Vulcanol. 5, 179-186.

Falsaperla, S., Langer, H., Spampinato, S., 1998. Statistical analyses and characteristics of volcanic tremor on Stromboli Volcano (Italy). Bull. Volcanol. 60(2), 75-88.

Federico, C., Brusca, L., Carapezza, M.L., Cigolini, C., Inguaggiato, S., Rizzo, A., Rouwet, D., 2008. Geochemical evidences of the incoming 2002-03 Stromboli eruption: variations in CO_2 and Rn emissions and helium and carbon isotopes. AGU Geophysics Monograph Series 182, 117-128.

Finizola, A., Sortino, F., Lenat, J.F., Valenza, M., 2002. Fluid circulation at Stromboli volcano (Aeolian Islands, Italy) from self-potential and CO_2 surveys. J. Volcanol. Geoth. Res. 116, 1-18.

Finizola, A., Sortino F.,·Lénat, J.F., Aubert, M., Ripepe M., Valenza, M., 2003. The summit hydrothermal system of Stromboli. New insights from self-potential, temperature, CO_2 and fumarolic fluid measurements, with structural and monitoring implications. Bull. Volcanol. 65, 486–504. doi:10.1007/s00445-003-0276-z.

Finizola, A., Aubert, M., Revil, A., Schütze, C., Sortino, F., 2009. Importance of structural history in the summit area of Stromboli during the 2002-2003 eruptive crisis inferred from temperature, soil CO2, self-potential, and electrical resistivity tomography. J. Volcanol. Geoth. Res. 183(3-4), 213-227.

Freeze, R.A., Cherry, J.A. 1979. Groundwater. Prentice-Hall Inc Englewood Cliffs NJ, pp. 604.

Gauthier, P.J., Condomines, C. 1999. ^{210}Pb-^{226}Ra radioactive disequilibria in recent lavas and radon degassing: inferences on the magma chamber dynamics at Stromboli and Merapi volcanoes. Earth Planet. Sci. Lett. 172, 111-126.

Gervino, G., Cigolini, C., Lavagno, A., Marino, C., Prati, P., Pruiti, L., Zangari, G., 2004. Modelling temperature distributions and radon emission at Stromboli Volcano using a non-extensive statistical approach. Physica A 340(1-3), 402-409.

Giammanco, S., Sims, K.W., Neri, M., 2007. Measurements of ^{220}Rn and ^{222}Rn and CO_2 emissions in soil and fumarole gases on Mt. Etna Volcano (Italy): implications for gas transport and shallow ground fracture. Geochem. Geophys. Geosyst. 8, Q10001. doi:10.1029/2007GC001644.

Gillot, P.Y., Keller, J., 1993. Radiochronogical dating of Stromboli. Acta Vulcanol. 3, 69-77.

Gilmore, G.K., Phillips, P., Denaman, A., Sperinn, M., Pearce, G., 2001. Radon levels in abandoned metalliferous mines, Devon, Southwest England. Ecotox. Environ. Safe. 49, 281-292.

Gründel, M., Postendörfer. J., 2003. Characterization of an electronic Radon gas personal Dosimeter. Rad. Prot. Dosim. 107(4), 287–292.

Harris, A.J.L., Ripepe, M., 2007. Temperature and Dynamics of Degassing at Stromboli. J. Geophys. Res. 112. doi:1029/2006JB0004393.

Harris, A.J.L., Dehn, J., Patrick, M.R., Calvari, S., Ripepe, M., Lodato, L., 2005. Lava effusion rates from hand-held thermal infrared imagery: an example from the June 2003 effusive activity at Stromboli. Bull. Volcanol. 68, 107–117.

Heiligmann, M., Stix, J., Williams-Jones, G., Lollar, B.S., Garzon, G. V., 1997. Distal degassing of radon and carbon dioxide on Galeras volcano. J. Volcanol. Geotherm. Res. 77, 267-283.

Hernandez, P., Perez, N., Salazar, J., Reimer, M., Notsu, K., Wakita, H. 2004. Radon and helium in soil gases at Cañadas caldera, Tenerife, Canary Islands, Spain. J. Volcanol. Geotherm. Res. 131, 59-76.

Holloway, J.R., 1977. Fugacity and activity of molecular species in supercritical fluids. In: Fraser DG (Eds) Thermodynamics in geology. Reidel Dordrecht, Holland, pp 161–181.

Inguaggiato, S., Vita, F., Rouwet, D., Bobrowski, N., Morici, S., Sollami, A., 2011. Geo-chemical evidence of the renewal of volcanic activity inferred from CO2 soil and SO2 plume fluxes: the 2007 Stromboli eruption (Italy). Bull. Volcanol. http://dx.doi.org/10.1007/s00445-010-0442-z.
.
INGV Report, 2011. In Rapporti di Vulcanologia: "Sopralluogo a Stromboli del 2 agosto 2011". Available at http://www.ct.ingv.it/2011.

Kotrappa, P., Dempsey, J.C., Stieff, L.R., 1993. Recent advances in electret ion chamber technology. Rad. Prot. Dosim. 47: 461-464.

Laiolo, M., Cigolini, C., Coppola, D., Piscopo, D., 2012. Developments in real-time radon monitoring at Stromboli volcano. J. Environm. Radioact. 105, 21-29.

Lapwood, E.R., 1948. Convection of a fluid in a porous medium. Proc. Cambridge Philos. Soc. 44, 508–52.

Lemmon, E.W., McLinden, M.O., Friend, D.G., 2005. Thermophysical properties of fluid systems. In: Linstrom PJ, Mallard WG (Eds) NIST Chemistry WebBook. NIST Standard Reference Database N 69, National Institute of Standards and Technology, Gaithersburg MD, 20899.

Longobardi, M., D'Auria, L., Esposito, M.A., 2012. Relative location of hybrid events at Stromboli Volcano, Italy. Acta Vulcanol. 24(1-2), 39-42.

Martini, M., Buccianti, A., Capaccioni, B., Giannini, L., Prati, F., 1996. Fumarole gas analysis (Stromboli). Acta Vulcanol. 6, 53-54.

Marchetti, E., Ripepe, M., 2005. Stability of the seismic source during effusive and explosive activity at Stromboli Volcano. Geophys. Res. Lett. 32, L03307. doi:10.1029/2004GL021406.

Métrich, N., Bertagnini, A., Di Muro, A., 2010. Conditions of magma storage, degassing and ascent at Stromboli: New insights into the volcano plumbing system with inferences on the eruptive dynamics. J. Petrol. 51(3), 603-626.

Neri, M., Behncke, B., Burton, M., Giammanco, S., Pecora, E., Privitera, E., Reitano, D., 2006. Continuous soil radon monitoring during the July 2006 Etna eruption. Geophys. Res. Lett. 33, L24316. doi:10.1029/2006GL028394.

Neri, M., Lanzafame, G., 2009. Structural features of the 2007 Stromboli eruption. J. Volcanol. Geoth. Res. 182(3-4), 137-144. doi:10.1016/j.jvolgeores.2008.07.021.

Newhall, C.G., Self, S., 1982. The volcanic explosivity index (VEI): An estimate of explosive magnitude for historical volcanism. J. Geophysic. Res. 87, 1231-1238.

Nikolopoulos, D., Vogiannis, E., Petraki, E., Zisos, A., Louiz, A., 2012. Investigation of the exposure to radon and progeny in the thermal spas of Loutraki (Attica-Greece): Results from measurements and modelling. Sci. Tot. Environm. 408-3, 495-504.

Padilla, G. D., et al. (2013), Soil gas radon emissions and volcanic activity at El Hierro (Canary Islands): The 2011-2012 submarine eruption, Geochem. Geophys. Geosyst., 14, 432–447, doi:10.1029/2012GC004375.

Padrón, E., Padilla, G., Hernández, P.A., Pérez, N.M., Calvo, D., Nolasco, D., Barrancos, J., Melián, G.V., Dionis, S., Rodríguez, F., 2013. Soil gas geochemistry in relation to eruptive fissures on Timanfaya volcano, Lanzarote Island (Canary Islands, Spain). J. Volcanol. Geotherm. Res. 250, 91–99.

Patrick, M.R., Harris, A.J.L., Ripepe, M., Dehn, J., Rothery, D.A., Calvari, S., 2007 Strombolian explosive styles and source conditions: insights from thermal (FLIR) video. Bull. Volcanol. 69, 769–784. doi:10 1007/s00445-006-0107-0.

Pérez, N.M., Hernández, P.A., Padrón, E., Melián, G., Marrero, R., Padilla, G., Barrancos, J., Nolasco, D., 2007. Precursory subsurface ^{222}Rn and ^{220}Rn degassing signatures of the 2004 seismic crisis at Tenerife, Canary Islands. Pure Appl. Geophys. 164, 2431-:2448.

Piboule, M., Pourchet, M., Bouchez, R., Amosse, J., Brenac, P., Maley, J., Pinglot, J.F.,Vincent, C., 1990. Radiometric studies of Lake Nyos (Cameroon) sediments: evidence of strong mixing and excess 210Pb. J. Volcanol. Geotherm. Res. 42(4), 363-372.

Pinault, J.L., Baubron, J.C., 1996. Signal processing of soil gas radon, atmospheric pressure and soil temperature data: a new approach for radon concentration modeling. J. Geophys. Res. 101, 3157-3171.

Pistolesi, M., Delle Donne, D., Pioli, L., Rosi, M., Ripepe, M., 2011. The 15 March 2007 explosive crisis at Stromboli volcano, Italy: Assessing physical parameters through a multidisciplinary approach. J. Geophys. Res. B Solid Earth 116(12), B12206.

Revil, A., Finizola, A., Ricci, T., Delcher, E., Peltier, A., Barde-Cabusson, S., Avard, G., Bailly, T., Bennati, L., Byrdina, S., Colonge, J., Di Gangi, F., Douillet, G., Lupi, M., Letort, J., Tsang Hin Sun, E., 2011. Hydrogeology of Stromboli volcano, Aeolian Islands (Italy) from the interpretation of resistivity tomograms, self-potential, soil temperature and soil CO_2 concentration measurements. Geophys. J. Int. 186, 1078–1094. doi: 10 1111/j 1365-246X 2011 05112 x.

Rinaldi, A.P., Vandemeulebrouck, J., Todesco, M., Viveiros, F., 2012. Effects of atmospheric conditions on surface diffuse degassing. J. Geophysic. Res. Solid Earth JB11201. doi:10.1029/2012JB009490.

Ripepe, M., Gordeev, E., 1999. Gas bubble dynamics model for shallow volcanic tremor at Stromboli. J. Geophys. Res. 104(B5), 10639-10654.

Ripepe, M., Marchetti, E., Ulivieri, G., Harris, A.J., Dehn, J., Burton, M., Caltabiano, T., Salerno, G., 2005. Effusive to explosive transition during the 2003 eruption of Stromboli volcano. Geology 33/5, 341-344.

Ripepe M., Marchetti E., Ulivieri G., 2007. Infrasonic Monitoring at Stromboli Volcano during the 2003 effusive eruption: insinghts on the explosive and degassing process of an open conduit system. J. Geophys. Res. 112, B09207, doi:10.1029/2006jB004613,2007.

Ripepe, M., Delle Donne, D., Lacanna, G., Marchetti, E., Ulivieri, G., 2009. The onset of the 2007 Stromboli effusive eruption recorded by an integrated geophysical network. J. Volcanol. Geotherm. Res. 182, 131-136.

Rizzo, A., Grassa, F., Inguaggiato, S., Liotta, M., Longo, M., Madonia, P., Brusca, L., Capasso, G., Moricia, S., Rouwet, D., Vita, F. 2009. Geochemical evaluation of observed changes in volcanic activity during the 2007 eruption at Stromboli (Italy). J. Volcanol. Geotherm. Res. 182, 246-254.

Robertson, E.C., Peck, D.L. 1969. Thermal conductivity of vesicular basalt. Eos Transact Am. Geophys. Un. 50(4), 339.

Rosi, M., Bertagnini, A., Landi, P., 2000. Onset of persisting activity at Stromboli Volcano (Italy). Bull. Volcanol. 62, 294-300.

Rosi, M., Bertagnini, A., Harris, A.J.L., Pioli, L., Pistolesi, M., Ripepe, M., 2006. A case history of paroxysmal explosion at Stromboli: timing and dynamics of the April 5, 2003 event. Earth Planet. Sci. Lett. 243, 594–606.

Segovia, N., Mena, M., Monnin, M., Peña, P., Seidel, J.L., Tamez, E., 1997. Radon in-soil variations related to volcanic activity. Radiat. Measurem. 28(I-6): 745-750.

Segovia, N., Mena, M., 1999. Soil radon pulses related to the initial phases to volcanic eruptions. Il Nuovo Cimento, 22C (3-4), 275-279.

Seidel, J.L., Monnin, M., Garcia, J.R., Ricard, L.P., Staudacher, T., 1999. Systematic radon survey over active volcanoes. Il Nuovo Cimento 22 C, 363-368.

Sinclair, A.J., 1974. Selection of thresholds in geochemical data using probability graphs. J. Geochem. Explor. 3, 1929-149.

Siniscalchi, A., Tripaldi, S., Neri, M., Giammanco, S., Piscitelli, S., Balasco, M., Behncke, B., Magrì, C., Naudet, V., Rizzo, E., 2010. Insights into fluid circulation across the Pernicana Fault (Mt. Etna, Italy) and implications for flank instability. Journal of Volcanology and Geothermal Research 193, 137–142.

Streil, T., Oeser, V., Feige, S., 2002. An electronic radon dosimeter as a multipurpose device-a bridge between dosimetry and monitoring. Geofisica Internacional 41, 285-288.

Su, C.C., Huh, C.A., 2002. Atmospheric Po-210 anomaly as a precursor of volcano eruptions. Geophys. Res. Lett. 29(5). doi 2001GL013856.

Thomas, D.M., Cox, M.E., Cuff, K.E., 1986. The association between ground gas radon variations and geologic activity in Hawaii. J. Geophys. Res. 91, 12186-12198.

Tibaldi, A., Corazzato, C., Marani, M., Gamberi, F., 2009. Subaerial-submarine evidence of structures feeding magma to Stromboli Volcano, Italy, and relations with edifice flank failure and creep. Tectonophys. 469(1-4), 112-136.

Tinti, S., Maramai, A., Armigliato, A., Graziani, L., Manucci, A., Pagnoni, G., Zaniboni, F., 2006. Observations of physical effects from tsunamis of December 30, 2002 at Stromboli volcano, southern Italy. Bull. Volcanol. 68, 450-461.

Varley, N.R., Armienta, M.A., 2001. The absence of diffuse degassing at Popocatepetl volcano, Mexico. Chem. Geol. 177, 157-173.

Ventura, G., Vilardo, G., 1999. Slip tendency analysis of the Vesuvius faults: Implications for the seismotectonic and volcanic hazard assessment. Geophys. Res. Lett. 26(21), 3229-3232.

Ventura, G., Vilardo, G., Milano, G., Pino, N.A. 1999. Relationships among crustal structure, volcanism and strike-slip tectonics in the Lipari-Vulcano volcanic complex (Aeolian Islands, Southern Tyrrhenian Sea, Italy). Phys. Earth Planet. Inter. 116, 31-52.

Viveiros, F., Ferreira, T., Cabral Vieira, J., Silva, C., Gaspar, J.L., 2008. Environmental influences on soil CO_2 degassing at Furnas and Fogo volcanoes (São Miguel Island, Azores archipelago). J. Volcanol. Geotherm. Res. 177(4), 883-893.

Williams-Jones, G., Stix, J., Heiligmann, M., Charland, A., Sherwood Lollar, B., Arner, N., Garzón, G.V., Barquero, J., Fernandez, E., 2000. A model of diffuse degassing at three subduction-related volcanoes. Bull. Volcanol. 62, 130-142.

Zimmer, M., Erzinger, J., 2003. Continuous H_2O, CO_2, ^{222}Rn and temperature measurements on Merapi Volcano,Indonesia, J. Volcanol. Geoth. Res. 125, 25-38.

Žunić, Z.S., Kobal, I., Vaupotič, J., Kozak, K., Mazur, J., Birovljev, A., Janik, M., Čeliković, I., Ujić, P., Demajo, A., Krstić, G., Jakupi, B., Quarto, M., Bochicchio, F., 2006. High natural radiation exposure in radon spa areas: a detailed field investigation in Niška Banja (Balkan region). J. Environm. Radioact. 89-3, 249-260.

Figure Captions

Fig. 1. a) the Aeolian islands and the regional tectonic setting. Red dotted lines represent the regional alignments; b) Digital Elevation Model (DEM) for Stromboli (Baldi et al, 2005) with the numbered stations for periodic radon measurements; the main structural features of the island are also reported (cf., Finizola et al., 2002; Tibaldi et al., 2009). Red and yellow stars represent the

location of the INGV geochemical summit station and the COA volcano observatory, respectively (see text for details).

Fig. 2. Probability plots for three selected stations of the network. Radon concentrations (measured with E-PERM® electretes) are plotted onto a logarithmic scale. Background, threshold and anomaly values (for all the stations of the network) were determined according to Sinclair (1974) (see Appendix A for details).

Fig. 3. Map of average radon emissions plotted onto Stromboli DEM that covers the whole island. Data were collected from November 2005 and September 2006 following the expansion of the network to 38 measuring sites.

Fig. 4. Maps of radon concentrations onto the NE sector of Stromboli during the typical Strombolian activity; a) October 2002 (cf., Cigolini et al., 2005); b) September 2005; c) February 2007 (cf., Cigolini et al., 2009; for the February-March 2007 data). On the right side of each panel we report the difference of the measured radon concentrations with the calculated threshold values (for all the stations of network; see Fig. 2 and Appendix A).

Fig. 5. Maps of radon concentrations recorded during the effusive eruptions of 2002-2003 and 2007; a) February 2003; b) March 2003 (before the paroxysmal explosion of April 5, 2003); c) March 2007 (integrated measurements during this time span also include the paroxysmal explosion of March 15, 2007).

Fig. 6. Timeseries of radon measurements obtained automatically during 2005-2007 at the summit station (PZZ, i.e., station 6 of the network). The sampling time is 4 hours. Dots represent single measurements whereas the thick curve is the daily average curve. The squares represents integrated

measurements with track-etch detectors during malfunctioning of the automatic radon dosimeter. In panels (b), (c) and (d) represent environmental parameters (atmospheric temperature and rainfall in mm are from the Stromboli volcano observatory, COA located at 90 m a.s.l.; cf. Fig. 1b) and the summit INGV station (atmospheric pressure; cf. Fig. 1b). Bars represent two major explosions: on August 5, 2005 and October 16, 2006, respectively. The light grey field refers to a period of intense local seismicity and high explosive activity (see Fig. 7 and text for details).

Fig. 7. Comparison of radon emissions recorded automatically (a) with selected geophysical parameters; b) seismic tremor; c) infrasonic puffing. Red curves represent the monthly averages. Bars represent two major explosions: on August 5, 2005 and October 16, 2006, respectively. The light grey field refers to a period of intense local seismicity that occurred during April 18 and May 5, 2006 (D'Auria et al., 2006). The dark grey field is the duration of the effusive eruption of 2007 (from February 27 to April 2, 2007).

Fig. 8. a) Sketch of the structural features and thermal anomalies of the summit area of the Stromboli volcano (simplified after Finizola et al., 2003; 2009). Location of radon stations and temporary radon measurement sites; b) and c) are selected images of the fracture zones where high to extremely high radon emissions (detected by means of E-PERM® electretes) have been recorded during January-February 2003 (see Table 3).

Fig. 9. Automatic measurements of very high radon emissions at selected sites during June-early July 2007; a) radon concentrations measured at the summit station (PZZ, station 6 of the network) expressed on a logarithmic scale; b) radon concentration at station 13 (located on the eastern sector along the N60°E fracture zone). Insets provide the location of the stations. Grey fields outline specific variations of their trends since June 20, 2007 (see text for details).

Fig. 10. Comparison of the timeseries of radon and thoron data collected during June-early July 2007, at PZZ station (cf. Fig. 9a). The use of the logarithmic scale allow to better visualize the drastic changes in the concentrations of the two radiogenic isotopes. The sampling time is of 4 hours.

Fig. 1

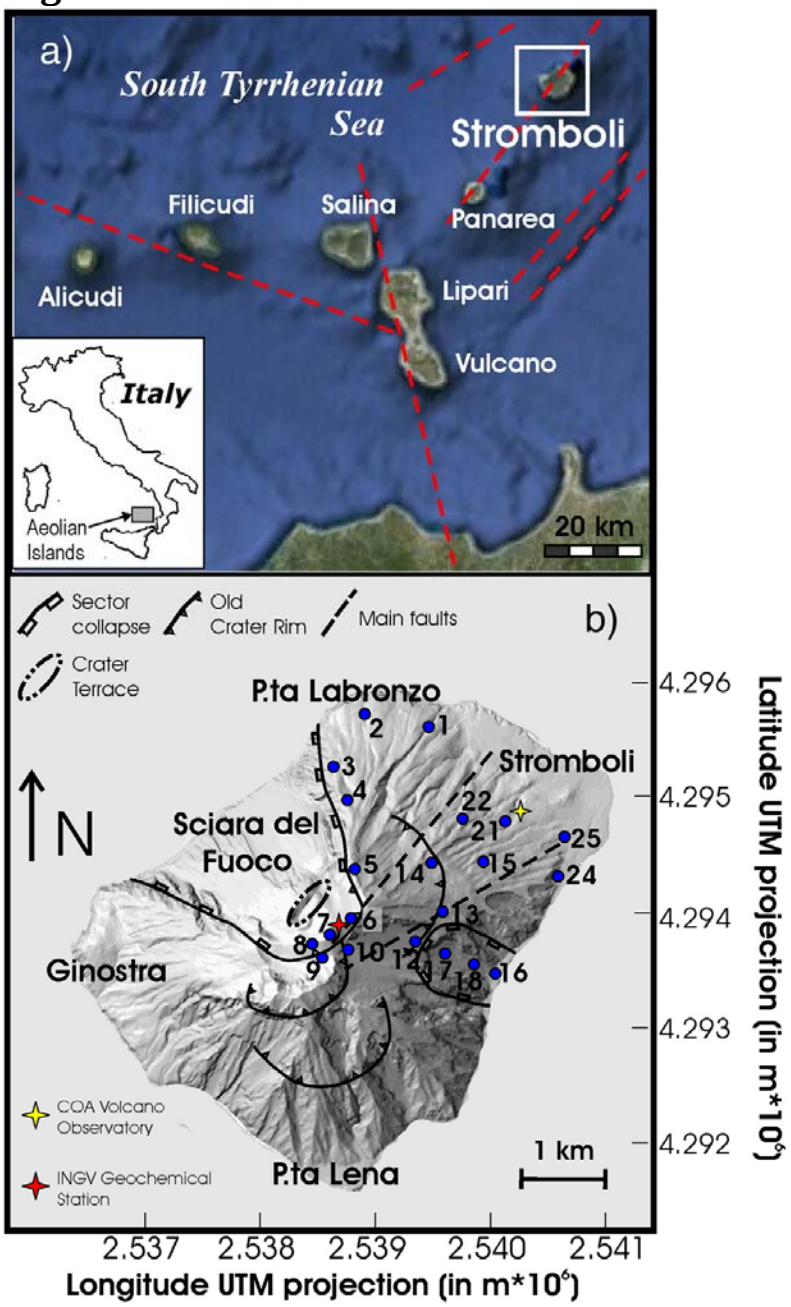

Fig. 2

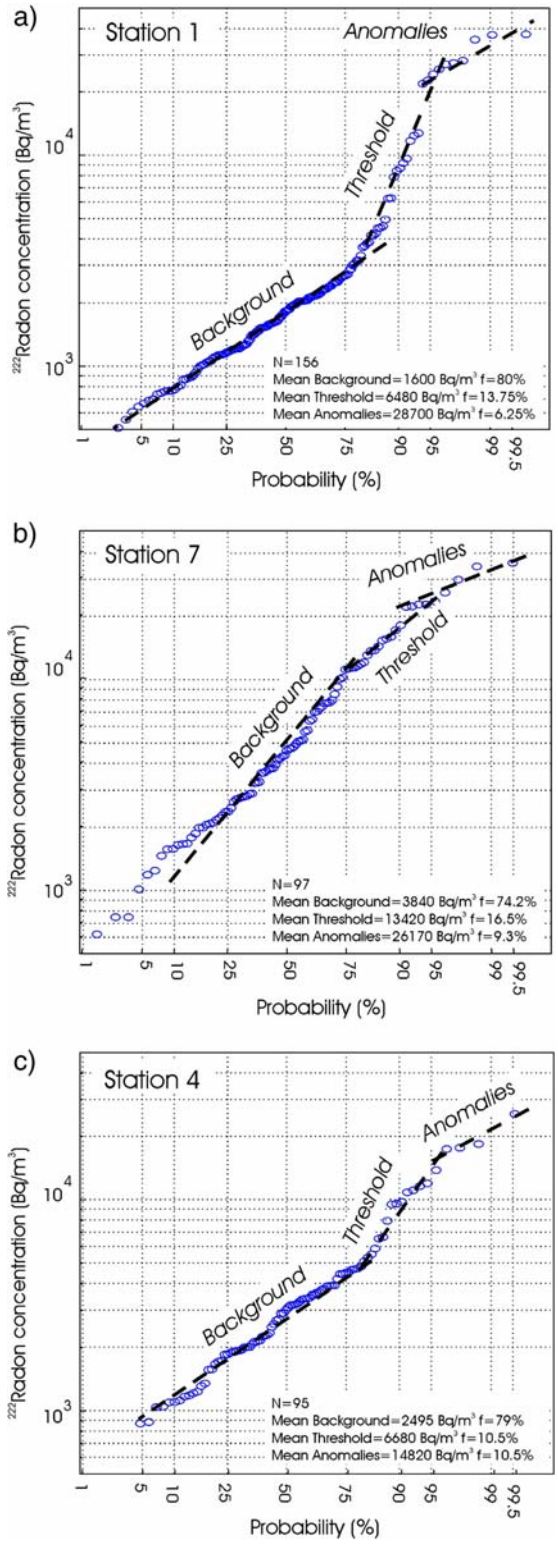
a)
Station 1
Anomalies
Threshold
Background
N=156
Mean Background=1600 Bq/m³ f=80%
Mean Threshold=6480 Bq/m³ f=13.75%
Mean Anomalies=28700 Bq/m³ f=6.25%
222Radon concentration (Bq/m³)
Probability (%)
b)
Station 7
Anomalies
Threshold
Background
N=97
Mean Background=3840 Bq/m³ f=74.2%
Mean Threshold=13420 Bq/m³ f=16.5%
Mean Anomalies=26170 Bq/m³ f=9.3%
222Radon concentration (Bq/m³)
Probability (%)
c)
Station 4
Anomalies
Threshold
Background
N=95
Mean Background=2495 Bq/m³ f=79%
Mean Threshold=6680 Bq/m³ f=10.5%
Mean Anomalies=14820 Bq/m³ f=10.5%
222Radon concentration (Bq/m³)
Probability (%)

Fig. 3

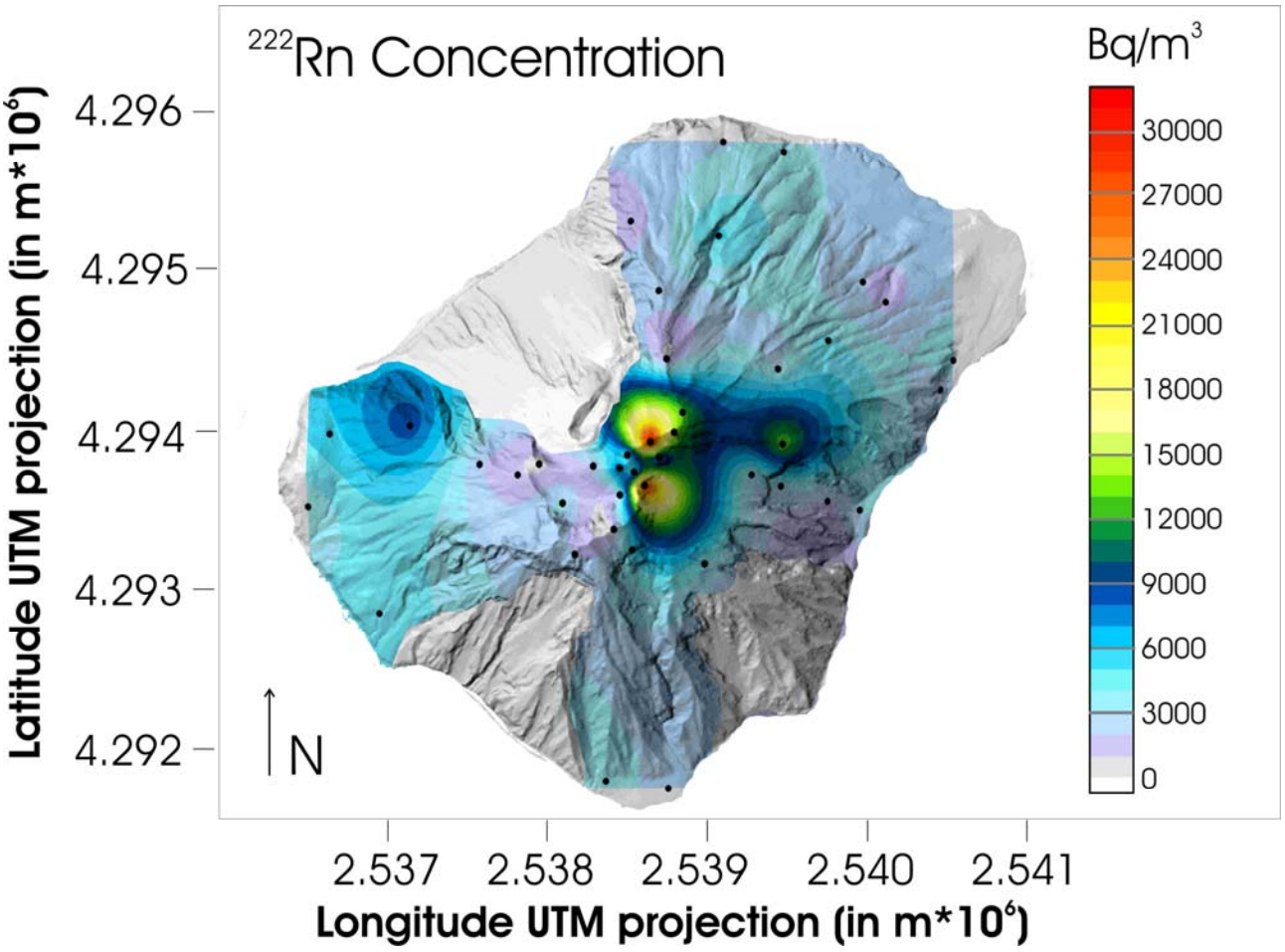
222Rn Concentration
Bq/m3
30000
27000
24000
21000
18000
15000
12000
9000
6000
3000
0
N
Latitude UTM projection (in m*10⁶)
4.296
4.295
4.294
4.293
4.292
2.537
2.538
2.539
2.540
2.541
Longitude UTM projection (in m*10⁶)

Fig. 4

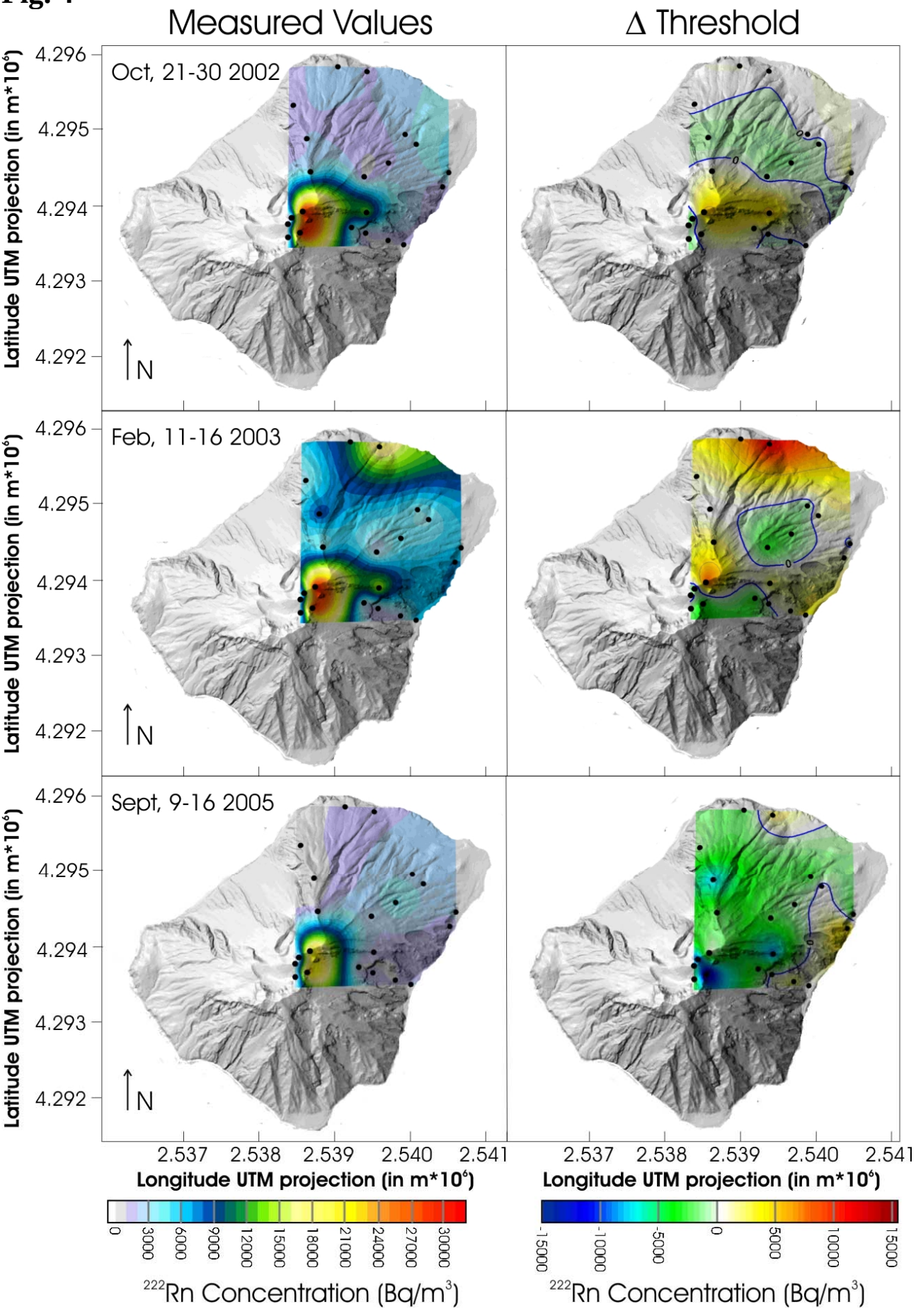
Measured Values
Δ Threshold
Oct, 21-30 2002
Feb, 11-16 2003
Sept, 9-16 2005
N
Latitude UTM projection (in m*10⁶)
4.296
4.295
4.294
4.293
4.292
2.537
2.538
2.539
2.540
2.541
Longitude UTM projection (in m*10⁶)
0
3000
6000
9000
12000
15000
18000
21000
24000
27000
30000
-15000
-10000
-5000
0
5000
10000
15000
222Rn Concentration (Bq/m3)

Fig. 5

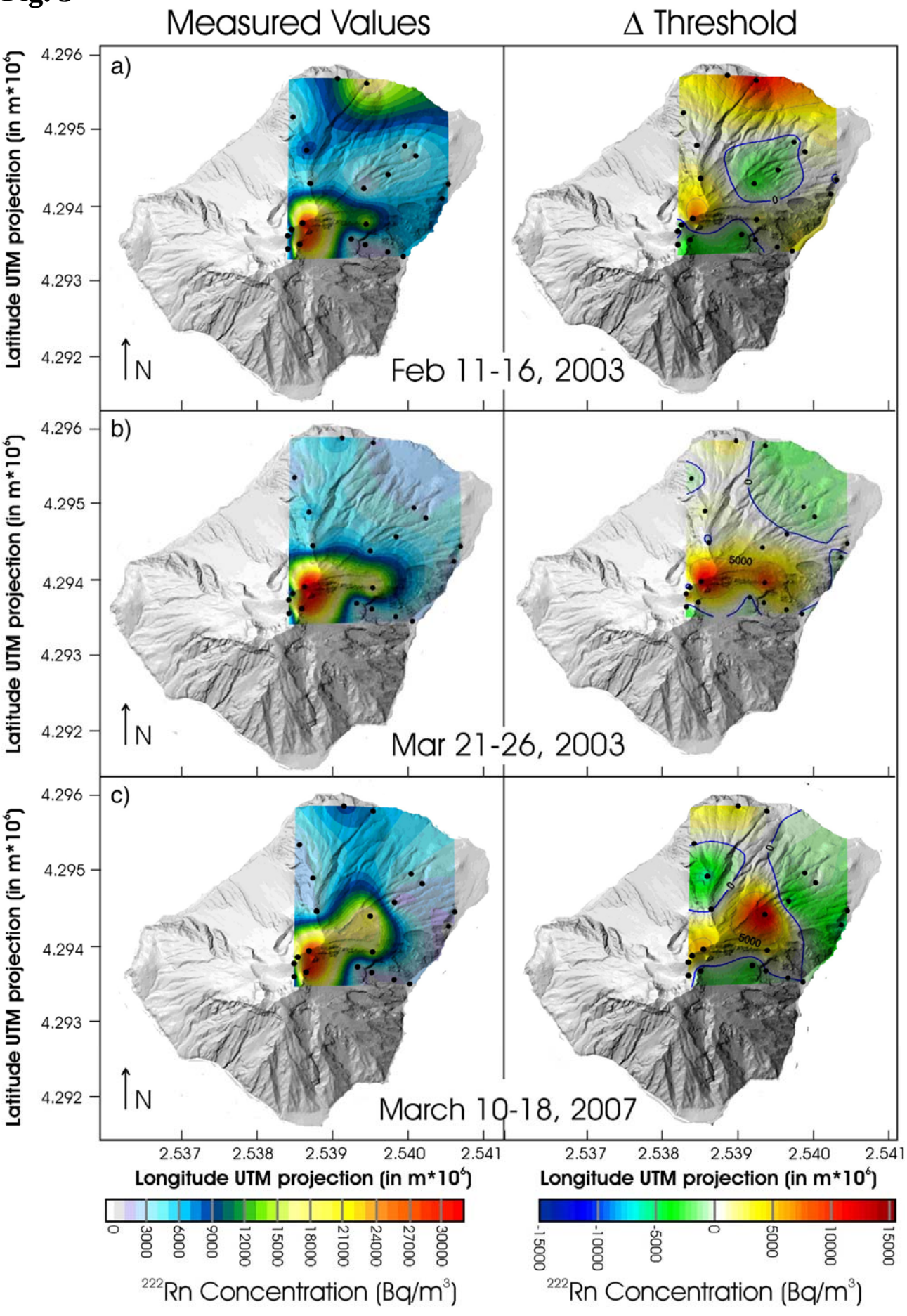
Measured Values
Δ Threshold
a)
b)
c)
Feb 11-16, 2003
Mar 21-26, 2003
March 10-18, 2007
N
0
5000
Latitude UTM projection (in m*10⁶)
4.296
4.295
4.294
4.293
4.292
2.537
2.538
2.539
2.540
2.541
Longitude UTM projection (in m*10⁶)
0
3000
6000
9000
12000
15000
18000
21000
24000
27000
30000
-15000
-10000
-5000
0
5000
10000
15000
222Rn Concentration (Bq/m3)

Fig. 6

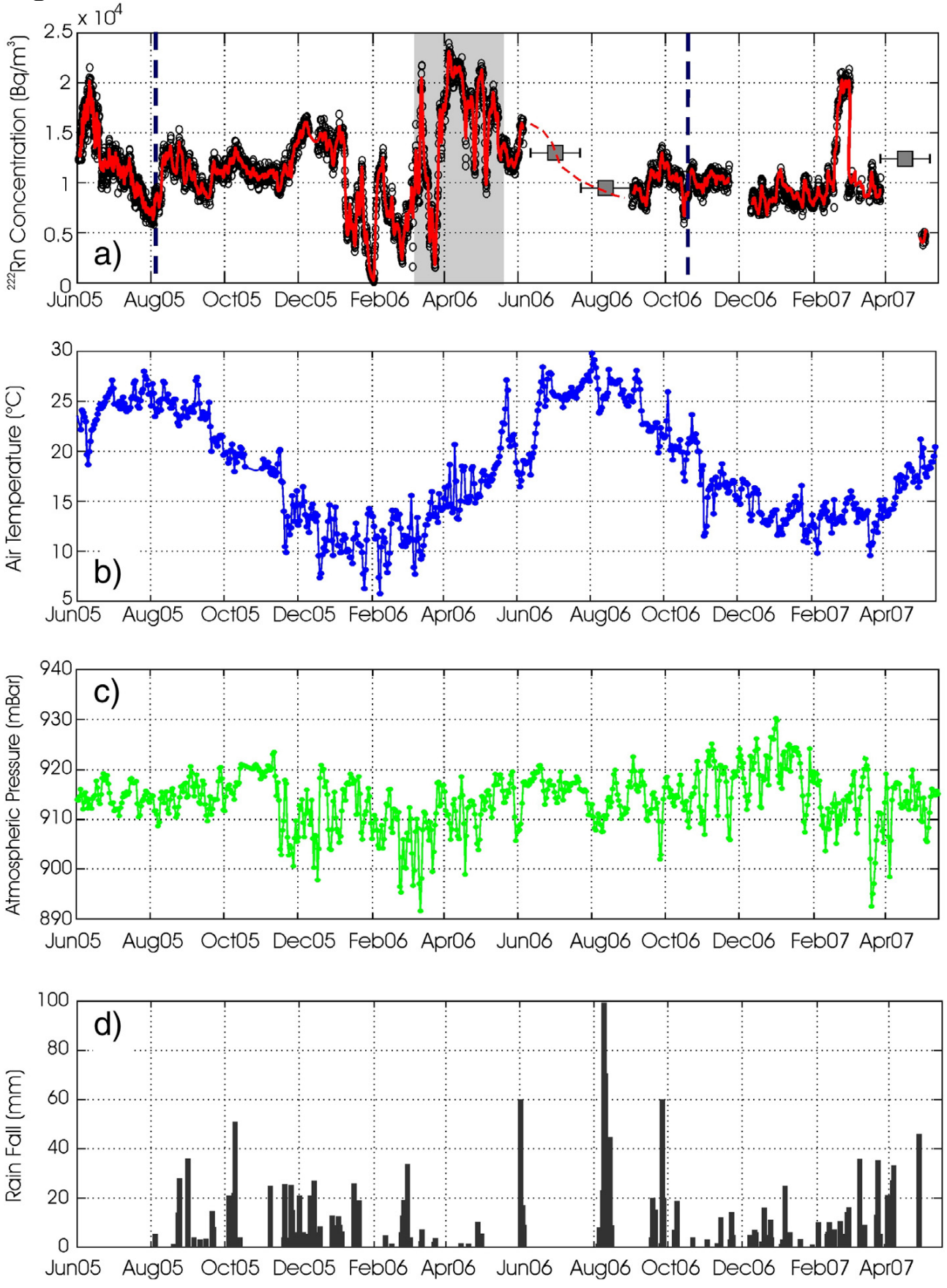
x 10^4
222Rn Concentration (Bq/m3)
a)
Air Temperature (°C)
b)
Atmospheric Pressure (mBar)
c)
Rain Fall (mm)
d)
Jun05 Aug05 Oct05 Dec05 Feb06 Apr06 Jun06 Aug06 Oct06 Dec06 Feb07 Apr07

Fig. 7

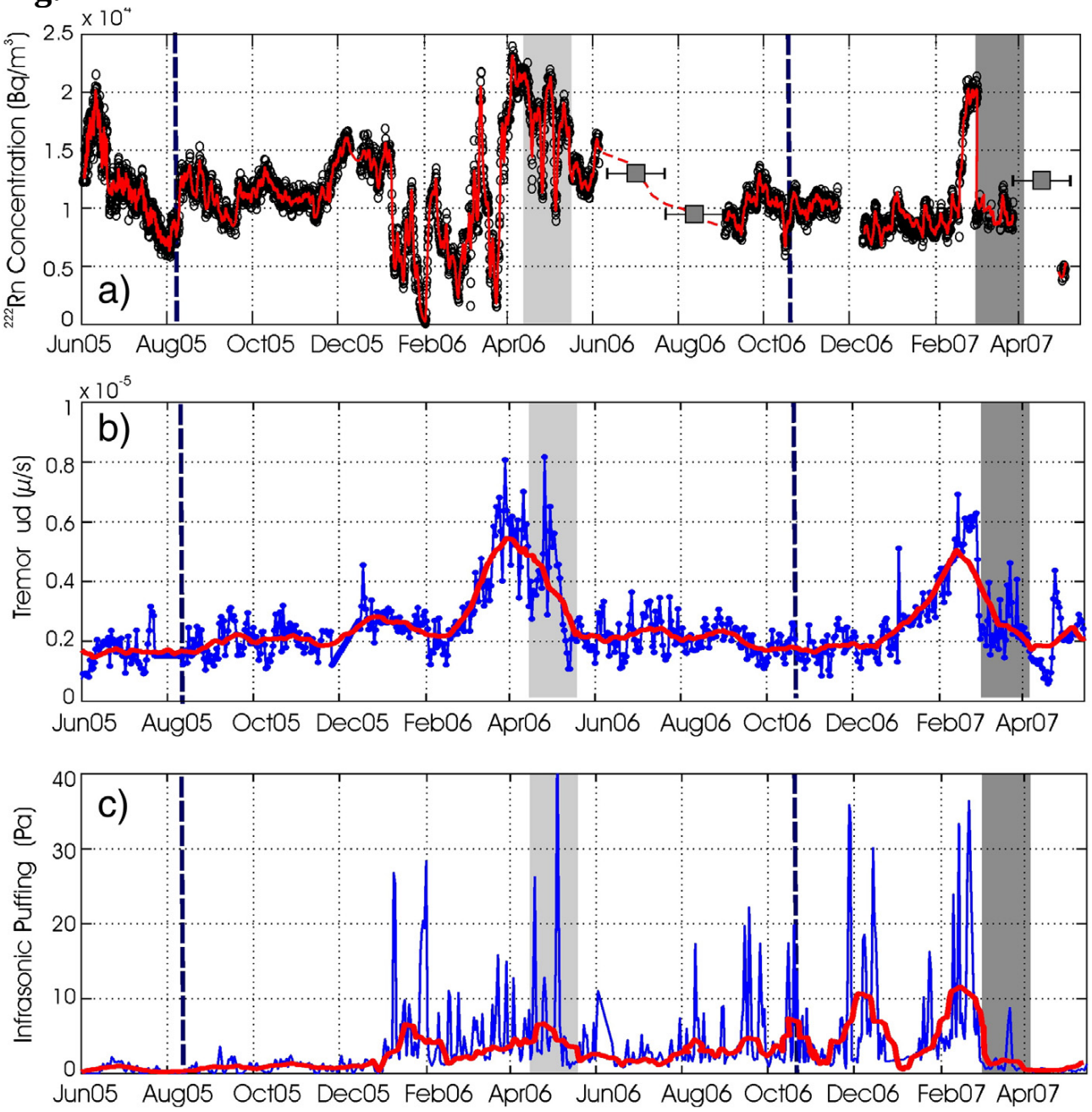
x 10⁻⁴
222Rn Concentration (Bq/m3)
2.5
2
1.5
1
0.5
0
a)
Jun05 Aug05 Oct05 Dec05 Feb06 Apr06 Jun06 Aug06 Oct06 Dec06 Feb07 Apr07
x 10⁻⁵
Tremor ud (μ/s)
1
0.8
0.6
0.4
0.2
0
b)
Jun05 Aug05 Oct05 Dec05 Feb06 Apr06 Jun06 Aug06 Oct06 Dec06 Feb07 Apr07
Infrasonic Puffing (Pa)
40
30
20
10
0
c)
Jun05 Aug05 Oct05 Dec05 Feb06 Apr06 Jun06 Aug06 Oct06 Dec06 Feb07 Apr07

Fig. 8

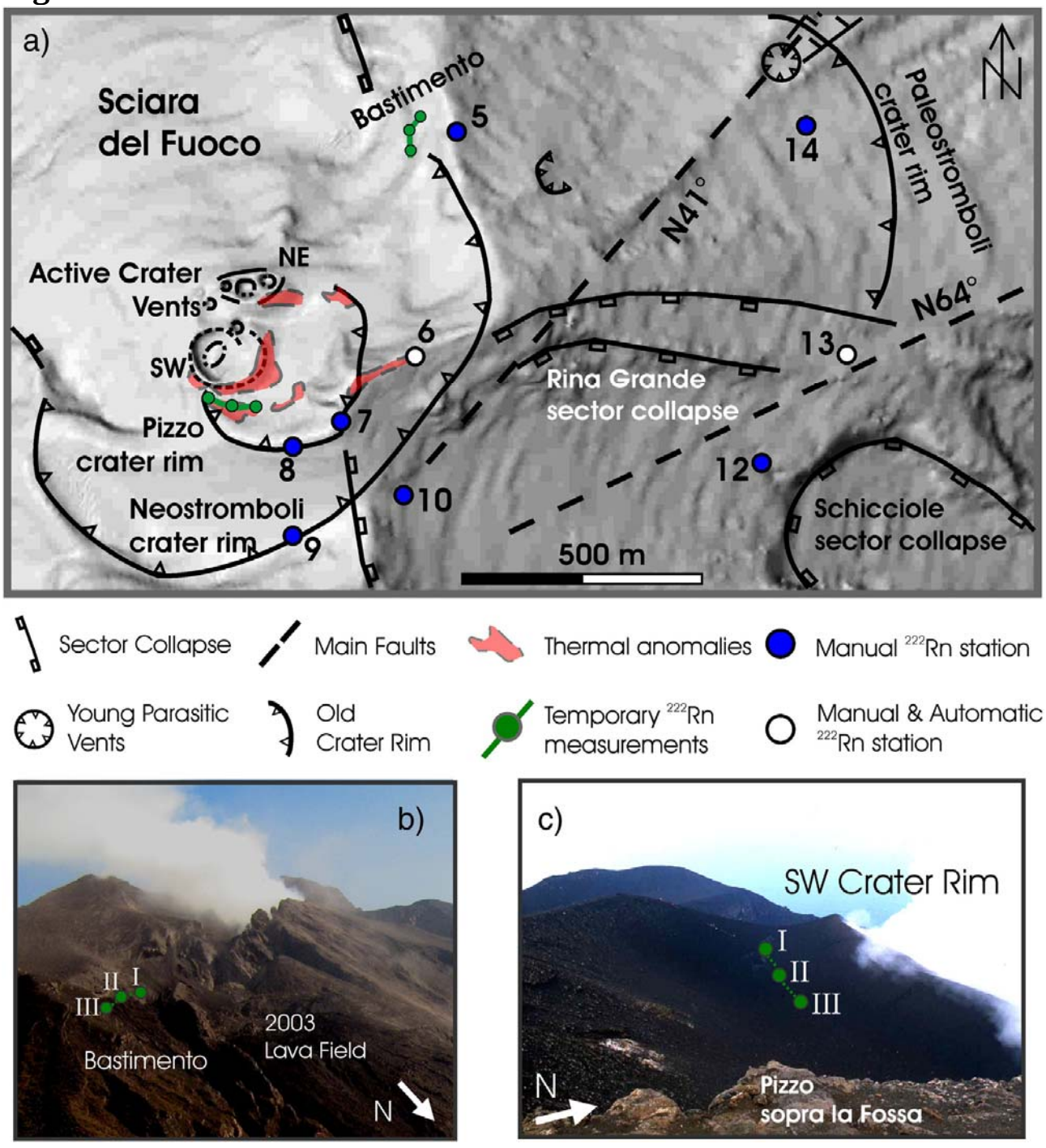
a)
Sciara del Fuoco
Bastimento
5
14
Paleostromboli crater rim
N41°
N64°
Active Crater Vents
NE
SW
6
13
Rina Grande sector collapse
Pizzo crater rim
7
8
12
10
Neostromboli crater rim
9
Schicciole sector collapse
500 m
Sector Collapse
Main Faults
Thermal anomalies
Manual 222Rn station
Young Parasitic Vents
Old Crater Rim
Temporary 222Rn measurements
Manual & Automatic 222Rn station
b)
II
I
III
2003 Lava Field
Bastimento
N
c)
SW Crater Rim
I
II
III
N
Pizzo sopra la Fossa

Fig. 9

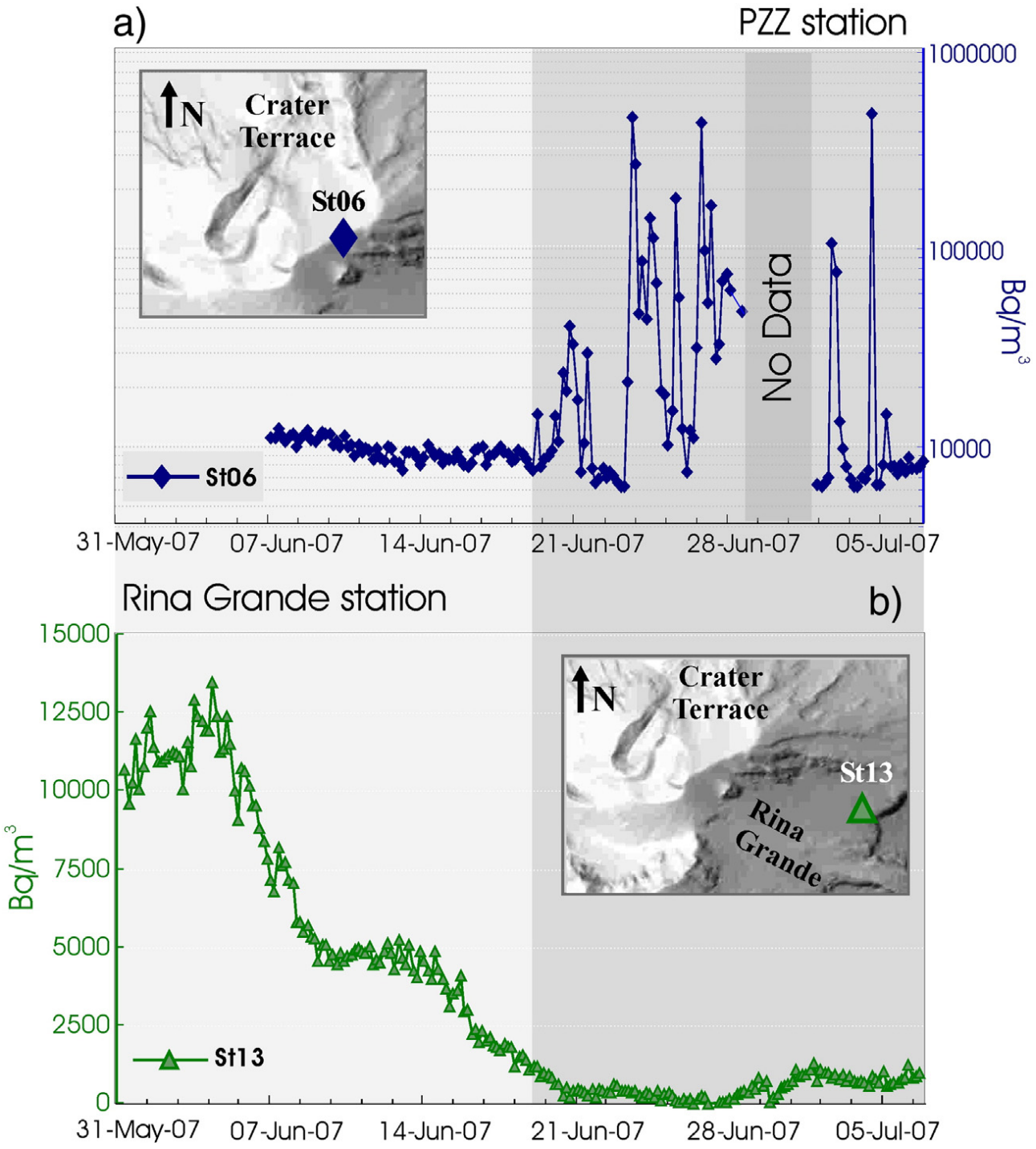
a)
PZZ station
N
Crater
Terrace
St06
No Data
St06
1000000
100000
10000
Bq/m3
31-May-07
07-Jun-07
14-Jun-07
21-Jun-07
28-Jun-07
05-Jul-07
Rina Grande station
b)
15000
12500
10000
7500
5000
2500
0
Bq/m3
N
Crater
Terrace
St13
Rina
Grande
St13
31-May-07
07-Jun-07
14-Jun-07
21-Jun-07
28-Jun-07
05-Jul-07

Fig. 10

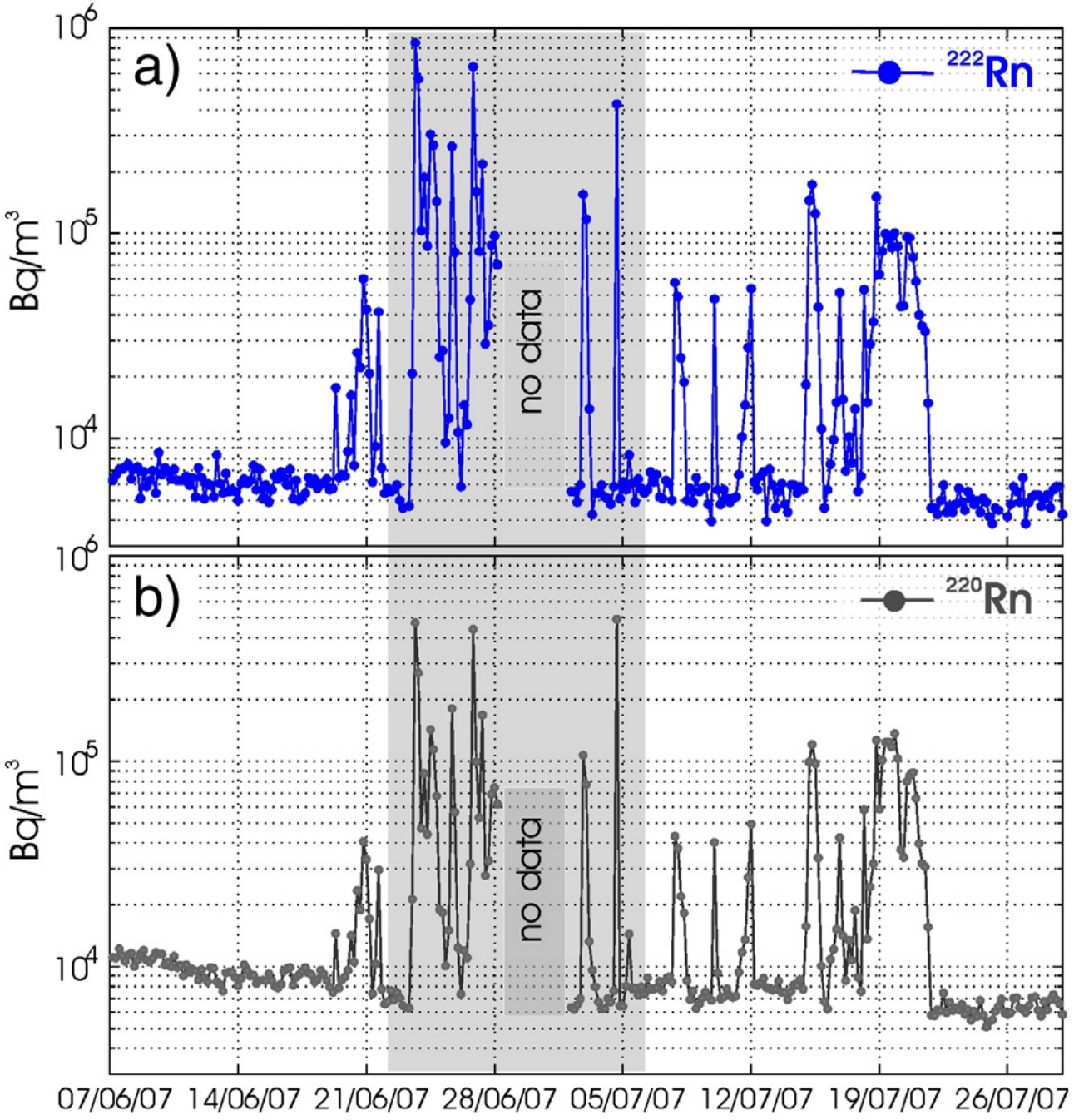
a)
^{222}Rn
no data
Bq/m^3
10^6
10^5
10^4
b)
^{220}Rn
no data
Bq/m^3
10^6
10^5
10^4
07/06/07
14/06/07
21/06/07
28/06/07
05/07/07
12/07/07
19/07/07
26/07/07

Table 1 - Summary of the in-soil radon concentrations measured in volcanic areas by using different techniques. Values are expressed in kBq/m^3

Volcano	Description	Period	Mean	Min	Max	Methods	References
Arenal (Costa Rica)	Network - 20 stations	1995	0.22 - 1.3	0.1	2.55	E-Perm®	Williams-Jones et al., 2000
Canadas Caldera (Tenerife - Spain)	Network - 356 measuring sites	1992/1995	5.5	0.03	73	Kodak LR115 Film	Hernandez et al. 2004
Cerro Negro (Nicaragua)	Network - 29 stations	1994-1996	0.35	0.3	26.7	E-Perm®	Connors et al. 1996
El Chichon (Mexico)	Monitoring Network	1982	0.6	NR	13.5	Kodak LR115 Film	Segovia et al. 1999
Galeras (Colombia)	Network - 23 measurement site	1993-1994	18	0.4	50	E-Perm®	Heiligman et al. 1997
Irazu (Costa Rica)	3 monitoring stations	Nov 1994	2-14	0	35	Barasol (ALGADE)	Seidel et al. 1999
Kilauea (Hawaii - USA)	Network - 10 stations	1981-1984	NR	0.1	12	Kodak LR115 Film	Thomas et al. 1986
Merapi (Indonesia)	Woro Fumarole Multiparametric Station	Jul-2000	NR	4	15	Radon Alpha-Scintillometer	Zimmer & Ernzinger 2003
Mt. Etna (Italy)	18 Measurement Sites	2005-2006	10.4	0.23	104	RAD7 (Durridge)	Giammanco et al. 2007
	NS profile across Pernicana Fault	Oct 2006	NR	1	5	RAD7 (Durridge)	Siniscalchi et al. 2010
	Southern Flank (3 Profiles)	2008-2009	2.7	0.03	11.6	RAD7 (Durridge)	Bonforte et al., 2012
Mt. Vesuvius (Italy)	Network - 20 Stations	1998 - 1999	4	0.4	35	Charcoal Cannister	Cigolini et al. 2001
Piton de la Fournaise	Pas de Bellecombe	1994-1997	0.3	0.1	2	Clipperton II	Seidel et al. 1999
(Reunion Island)	Dolomieu - Souffriere Sites	1994-1995	NR	0	40	Clipperton II	Segovia et al. 1997
Poas (Costa Rica)	7 monitoring stations	1982-1992	6	NR	24	Kodak LR115 Film	Segovia et al. 1999
Popocatepetl (Mexico)	Network - 667 sites	1997-1999	4.65	0	35	PYLON AB-5	Varley and Armienta, 2001
Stromboli (Italy)	Network - 21 Stations	2002 - 2007	5.5	0.12	63.4	E-Perm®	this work
St. Miguel (El Salvador)	Network - 205 sites	1999-2000	4.1	0.08	31	PYLON AB-5	Cartagena et al. 2004
Villarrica (Chile)	Network - 13 measurement sites	Nov-2004	1.6	0.4	6.2	E-Perm®	Cigolini et al., 2013

NR - Not Reported

Table 2 - Summary of very high and extremely high radon emissions measured during the 2002-2003 effusive event,along the fractures that rim the SW crater and crosscut the Bastimento site.

Time	Sites	*Vi*	*Vf*	*Exp Time* *hour*	^{222}Rn *Bq/m^3*
	SW Crater Rim				
14-Jan-2003	Point 1	403	384	1.633	71,528
14-Jan-2003	Point 2	725	320	1.683	1,479,607
14-Jan-2003	Point 3	153	146	1.667	25,818
	SW Crater Rim				
15-Jan-2003	Point 1	725	715	1.800	34,155
15-Jan-2003	Point 2	717	677	1.783	137,930
15-Jan-2003	Point 3	728	678	1.733	177,389
	SW Crater Rim				
08-Feb-2003	Point 1	623	587	0.517	428,494
08-Feb-2003	Point 2	654	652	0.517	23,795
	SW Crater Rim				
09-Feb-2003	Point 1	384	380	0.667	36,888
09-Feb-2003	Point 3	587	428	0.700	1,396,881
	Bastimento				
11-Feb-2003	Point 1	545	538	0.667	64,562
11-Feb-2003	Point 2	429	394	0.583	368,980
	SW Crater Rim				
12-Feb-2003	Point 1	744	593	0.583	1,591,919
12-Feb-2003	Point 2	730	714	0.550	178,893
12-Feb-2003	Point 3	721	717	0.517	47,601
	Bastimento				
12-Feb-2003	Point 1	594	582	0.450	163,985
12-Feb-2003	Point 2	667	665	0.450	27,322
12-Feb-2003	Point 3	694	689	0.450	68,321
	Bastimento				
13-Feb-2003	Point 1	667	661	0.333	110,686
13-Feb-2003	Point 2	730	708	0.350	386,550
13-Feb-2003	Point 3	694	649	0.367	754,742

Values reported of the initial and final voltages (Vi and Vf, respectively) and the exposure time (Exp Time) have been used to calculate ^{222}Rn concentrations (cf. Kotrappa et al., 1993).

Table A.1 - Average and range values for background, threshold and anomalous classes for each stations, of the network Following the method proposed by Sinclair (1974).

Station	Latitude	Longitude	Samples	Background		Threshold		Anomalous	
				mean	*range*	mean	*range*	mean	*range*
	UTM - WGS84	UTM - WGS84	no.	Bq/m^3		Bq/m^3		Bq/m^3	
St1	519538	429567	159	1596	*225-3159*	6482	*3332-12731*	28750	*21885-37612*
St2	519148	429573	168	2458	*500-5790*	7681	*6455-9344*	17662	*10201-36746*
St3	518566	429520	133	1140	*238-2543*	4734	*2711-10659*	20500	*14800-26706*
St4	518738	429475	95	2498	*400-4721*	6682	*4823-9580*	14816	*9776-25561*
St5	518782	429432	79	2143	*158-4981*	8257	*5725-10097*	15860	*11909-24080*
St6	518691	429382	101	15332	*1527-27504*	29314	*28437-29926*	33755	*30330-43777*
St7	518552	429375	97	3843	*293-10079*	13415	*11012-17837*	26169	*21812-35205*
St8	518511	429367	96	1746	*238-3873*	7760	*4909-13184*	41871	*31635-51661*
St9	518510	429350	95	1525	*243-4866*	7778	*6036-10431*	15080	*12976-18968*
St10	518655	429356	99	19115	*1379-30891*	33988	*31087-38627*	50323	*41365-63428*
St12	519500	429381	95	1803	*163-4510*	6605	*5003-8190*	14274	*11711-18040*
St13	519471	429427	96	3210	*152-10558*	14728	*11750-17798*	25008	*18590-41978*
St14	519795	429445	97	1245	*150-5856*	7678	*6198-9279*	24754	*16043-34776*
St15	520027	429338	98	2244	*400-4873*	7818	*5608-11828*	24132	*17179-35675*
St16	519496	429354	85	1492	*267-2660*	3475	*2870-4136*	11657	*4776-20363*
St17	519807	429344	53	967	*163-1586*	2031	*1715-2285*	4817	*4082-5190*
St18	520176	429471	51	1093	*155-1414*	2233	*1595-2233*	3382	*2631-3948*
St21	520032	429484	139	3144	*251-5119*	6752	*5370-9821*	27618	*12289-41168*
St22	520537	429415	127	2134	*400-3350*	4413	*3399-5638*	10759	*5900-25534*
St24	520622	429434	146	1255	*118-2673*	4227	*2719-6520*	13674	*7189-29278*
St25	519307	429362	156	2716	*409-4541*	6344	*4766-9507*	18173	*9885-26909*

Table B.1 - Summary of calculations for a convective cells geometries operating at the summit hydrothermal system of Stromboli. Densities (ρ_{fmix}) and thermal expansions (α_{fmix}) for fluid mixtures were calculated by using the MRK equation of Holloway (1977), whereas the average fluid viscosity (η_{fmix}) and the specific heats (C_{fmix}) of fluid mixtures were calculated according to the data of Lemmon et al. (2005). The above parameters were obtained at 6 and 10 MPa, respectively. Solutions were accepted when the lithostatic load at the depth H is $3 < P_{load} < 6$ MPa and $5 < P_{load} < 10$ MPa for LT and HT fluids, respectively (see text for details).

INPUT PARAMETERS

Parameters	Definitions	X_{CO_2}=0.9 at T=270 °C	X_{CO_2}=0.67 at T=410 °C	Units
η_{fmix}	Viscosity of the fluid mixture	$2*10^{-5}$	$2.5*10^{-5}$	Pa*s
ρ_{fmix}	Density of the fluid mixture	30	40	kg/m^3
α_{fmix}	Thermal expansion of the fluid mixture	$3*10^{-3}$	$2*10^{-3}$	$°C^{-1}$
ρ_m	Mean density (fluid-filled medium)	1800	2600	kg/m^3
C_{fmix}	Specific heat of the fluid mixture	$5*10^3$	$3*10^3$	J/kg*°C
k	Rock permeability	$1*10^{-12}$	$1*10^{-12}$	m^2
K	Rock thermal conductivity	2	2.8	Wm/°C
C_m	Specific heat (fluid-filled medium)	$1*10^3$	$1*10^3$	J/kg*°C

CALCULATED PARAMETERS*

Parameters	Definitions	X_{CO_2}=0.9 at T=270 °C	X_{CO_2}=0.67 at T=410 °C	Units
Ra	Rayleigh Number	254.016	447.749	adim
v_{fmix}	Velocity of the fluid miture	1193	1858	m/day
ϕ	porosity	10^{-4}	10^{-4}	adim
H	height of the convective cell	200	310	m

* - Δt_{total} = 0.167 days (i.e., a sampling time of 4 hours)